CHEMICALLY REACTING COUETTE FLOW WITH HYDROGEN INJECTION FOR TWO DIFFUSION MODELS

By

Randolph A. Graves, Jr.

Thesis submitted to the Graduate Faculty of the

Virginia Polytechnic Institute

in partial fulfillment for the degree of

MASTER OF SCIENCE

in

Mechanical Engineering

June 1969

CHEMICALLY REACTING COUETTE FLOW WITH HYDROGEN INJECTION FOR TWO DIFFUSION MODELS

By

Randolph A. Graves, Jr.

ABSTRACT

This investigation deals with an analytical study of the effects of hydrogen injection and chemical reaction on the flow properties of Couette flow with special emphasis given the diffusion model assumed for the calculations. The two diffusion models chosen for the present analysis are Fick's law diffusion and multicomponent diffusion. For most boundary layer and Couette flow analyses the approximate Fick's law diffusion model is used as it results in considerable mathematical and numerical simplification over the more exact but cumbersome multicomponent diffusion model. There is discussed in the literature the use of Couette flow to simulate the two-dimensional laminar boundary layer, however, there is no literature available concerning hydrogen injection into chemically reacting Couette flow with property variations nor is there literature available on the effect of the diffusion models used for the Couette flow solutions. The purpose of this study was to obtain solutions for the chemically reacting Couette flow with variable transport properties and hydrogen injection for the two diffusion models.

Solutions to the governing equations for Couette flow were obtained for the two diffusion models over a range of hydrogen injection rates. The results indicate that there are significant differences between the

solutions for the two diffusion models and these differences are manifested most in the concentration profiles and the lower wall heating rates.

CHEMICALLY REACTING COUETTE FLOW WITH HYDROGEN INJECTION FOR TWO DIFFUSION MODELS

By

Randolph A. Graves, Jr.

Thesis submitted to the Graduate Faculty of the

Virginia Polytechnic Institute

in partial fulfillment for the degree of

MASTER OF SCIENCE

in

Mechanical Engineering

APPROVED:

_____

Chairman, Dr. F. J. Pierce

_____ _____

Dr. J. Beverly Jones Dr. R. A. Comparin

June 1969

Blacksburg, Virginia

TABLE OF CONTENTS

ACKNOWLEDGMENTS

The author wishes to express his appreciation to the following people for their assistance in the preparation of this thesis: Mrs. Jean M. Foster, who assisted in the programing of the governing equations; Mrs. Nadine C. Kemper, who prepared the final figures for the thesis; Mrs. Margaret W. Sheppard, who typed the rough draft; Mrs. Yvonne B. Powell, who typed the final draft of this thesis; and to Dr. Felix J. Pierce, the author's thesis advisor, whose patience and encouragement provided the author with the necessary impetus to complete this study.

LIST OF FIGURES AND TABLES

FIGURE PAGE

TABLES

LIST OF SYMBOLS

C_f	nondimensional shear stress at lower wall
C_p	specific heat
C_{PR}	reactive specific heat, see equation (11)
$\mathcal{D}$	binary diffusion coefficient
D	Fick's law diffusion coefficient
D^T	thermal diffusion coefficient
F_b	body force
F	any function
h	static enthalpy
h_f^o	enthalpy of formation
K	mass fraction
K_p	equilibrium constant
M	molecular weight
$\overline{M}$	mixture molecular weight
n	number of moles
N	finite-difference station number
NT	total number of finite-difference stations
P	pressure
Q	heat transfer rate
q	nondimensional heat transfer rate
R	universal gas constant
s	distance between porous surfaces

T	temperature
u	flow velocity
U	dimensionless flow velocity
V	diffusion velocity
v	transverse or mass average velocity
X	mole fraction
y	coordinate normal to lower porous surface
δ_o	nondimensional mass addition rate
ϵ/K	nondimensional maximum energy of attraction
ζ_{ij}	number of atoms of element j in a molecule of species i
η	nondimensional coordinate
θ	nondimensional temperature
λ	thermal conductivity
μ	viscosity
ν	number of components
ρ	mass density
σ	collision diameter
$\Omega( )^*$	reduced collision integral
ω	species production rate
γ	nondimensional coordinate of reference 3, see equation (83)
α	coordinate parameter of reference 3, $\alpha = \int_o^\eta \frac{d\eta}{\mu}$
τ	shear stress

Subscripts

i	i^{th} species
j	j^{th} species
m	gaseous mixture
o	no injection
t	total
w	wall (lower porous surface)
∞	free stream (upper porous surface)
B.C.	boundary condition
CAL	calculated

Superscripts

~	"elemental"
°	reference condition
I	iteration number
J	iteration number

I. INTRODUCTION

The reduction of intense aerodynamic heating encountered by reentry and hypersonic flight vehicles through the use of mass transfer cooling has become widely accepted. Whether this mass transfer cooling is accomplished by ablation or transpiration, the gases injected into the boundary layer are generally quite different from the main stream flow. Since the heating reduction is greatest with low molecular weight gases, molecular hydrogen is usually a major component of the injected gases especially in the ablation of polymeric materials. The introduction of hydrogen into boundary-layer flow complicates the analysis as large property variations occur and molecular diffusion and chemical reactions must be considered.

In most analyses Fick's law diffusion is assumed as it is an easily applied approximation to the more exact but mathematically cumbersome multicomponent diffusion model. However, since the Fick's law diffusion model is an approximation the calculated diffusion velocities will be in error, especially when there are large differences in molecular weight of the diffusing species as is the case when hydrogen is present in an airstream. Thus a comparison of the diffusion models is necessary to provide an estimate of the errors incurred when using the approximate model.

In making a comparison of the diffusion models any simplification that can be used without concealing the important aspects of hydrogen injection into an air boundary layer is desirable. In the literature

the one-dimensional Couette flow model has been used to simulate the two-dimensional laminar boundary layer. However, the sources available consider only hydrogen injection into an air Couette flow with constant properties and no chemical reactions.

The present study is twofold in purpose: first the effects of hydrogen injection with property variations and chemical reactions will be considered and secondly comparisons will be made between two diffusion models. As in the literature, the one-dimensional Couette flow model will be used to simulate the two-dimensional laminar boundary layer. In this Couette flow representation the velocity of the moving plate represents the free-stream velocity, while the distance between the plates simulates the boundary-layer thickness.

This investigation was conducted under the auspices of the National Aeronautics and Space Administration at the Langley Research Center, Hampton, Virginia.

II. REVIEW OF LITERATURE

There exists surprisingly little information in the literature concerning the effects of the diffusion model on the solutions obtained for a chemically reacting airflow with hydrogen injection. There are no direct comparisons between the approximate Fick's law diffusion model and the more exact multicomponent diffusion model available from the literature, however, the analysis of Libby and Pierucci (ref. 1) does consider hydrogen injection into a laminar boundary layer with variable properties, chemical reactions and multicomponent diffusion, but these solutions are compared to rather limited constant property (Prandtl and Schmidt numbers equal to one) solutions, making the comparisons somewhat unrealistic and giving no insight into the effect of the diffusion model utilized. This thesis differs from the above analysis in several respects. First, the solutions for the approximate diffusion model analysis will employ the same assumptions as the multicomponent diffusion analysis, except for the diffusion model itself; and secondly, the present analysis uses the Couette flow model to simulate the two-dimensional laminar boundary layer.

There are several sources of information in the literature on hydrogen injection into Couette flow with the principal analysis being that of Eckert and Schneider (ref. 2), but because of the assumptions of no chemical reactions and constant properties their solutions are of only limited usefulness. A variable property analysis is given by Simon, et al. in reference 3 where hydrogen is injected into an inert stream with no chemical reactions. The present analysis differs from

these latter two references in that variable properties, chemical reactions, and two diffusion models are considered. Also, the present analysis will not employ the flame sheet approximation as did Libby and Pierucci to define combustion but instead a diffusion flame will result from the solution of the governing equations.

III. ANALYSIS

Figure 1 shows the Couette flow model. The lower porous surface, at $y = 0$, is stationary while the upper porous surface, at $y = s$, moves with a uniform velocity u_∞. The lower surface is at the temperature T_w and the upper surface at T_∞. The hydrogen gas, initially at temperature T_w, is injected perpendicularly into the flow uniformly through the stationary surface, and removed uniformly through the upper surface.

Basic Equations of Motion

The basic equations governing motion in a multicomponent chemically reacting gas are taken from Scala, reference 4. These equations are the continuity equation,

$$\frac{D\rho}{Dt} + \rho\nabla \cdot \vec{v} = 0 \tag{1}$$

and the momentum equation,

$$\rho \frac{D\vec{v}}{Dt} = \nabla \cdot \underset{\sim}{\pi} + \sum_i \rho_i F_{bi} \tag{2}$$

where $\underset{\sim}{\pi}$ is the pressure tensor,

and the energy equation,

$$\rho \frac{Dh}{Dt} = -\nabla Q + \Phi_D + \frac{DP}{Dt} + \sum_i \rho_i \vec{V}_i \vec{F}_{bi} \tag{3}$$

In this equation Q represents the energy flux due to temperature and concentration gradients and is given by

$$Q = -(\lambda \nabla T) + \sum_i \rho_i \vec{V}_i h_i$$

$$- \frac{RT}{n_t} \sum_i \sum_{j \neq i} \frac{n_j D_i^T}{M_i \mathcal{D}_{ij}} (\vec{V}_j - \vec{V}_i)$$

The viscous dissipation function Φ_D in equation (3) is given by the following relationship:

$$\Phi_D = \left\{ \frac{1}{2} \mu \sum_i \sum_j \left(\frac{\partial v_i}{\partial x_j} + \frac{\partial v_j}{\partial x_i} \right)^2 \right\} - \frac{2}{3} \mu \left(\sum_k \frac{\partial v_k}{\partial x_k} \right)^2$$

and finally there is the species continuity equation

$$\rho \frac{DK_i}{Dt} = \omega_i - \nabla \cdot (\rho_i \vec{V}_i) \qquad (4)$$

Assumptions for Present Analysis

For the present analysis the following assumptions are made:

1. The flow is steady.
2. The model is one dimensional.
3. Thermal diffusion effects are neglected.
4. Diffusion stress effects are neglected.
5. No body forces considered.

6. No pressure gradients.
7. No radiation heat transfer.
8. Chemical equilibrium exists throughout the flow.
9. Gas properties depend on local mixture concentration and temperature.
10. Both surfaces are impermeable to the main stream gas.
11. Prandtl's order of magnitude analysis is applicable (ref. 5).

Equations of Motion for Couette Flow

Using the above assumptions the basic governing equations of motion can be reduced to the following forms for Couette flow.

Continuity equation,

$$\frac{d(\rho v)}{dy} = 0 \tag{5}$$

momentum equation,

$$\rho v \frac{du}{dy} = \frac{d}{dy}\left(\mu \frac{du}{dy}\right) \tag{6}$$

energy equation,

$$\rho v \frac{dh}{dy} = \frac{d}{dy}\left(\lambda \frac{dT}{dy}\right) + \mu\left(\frac{du}{dy}\right)^2 - \frac{d}{dy}\left(\sum_i \rho_i V_i h_i\right) \tag{7}$$

species continuity equation,

$$\rho v \frac{dK_i}{dy} + \frac{d}{dy}(\rho_i V_i) = \omega_i \tag{8}$$

These equations are similar to the two-dimensional laminar boundary layer equations except for the Couette flow being one dimensional.

A further simplification of the energy equation can be obtained through the introduction of:

$$h = \sum_i h_i K_i$$

$$h_i = \int_{T^\circ}^{T} C_{Pi}\, dT + h_f^\circ \tag{9}$$

Thus

$$\frac{dh}{dy} = \sum_i K_i C_{Pi} \frac{dT}{dy} + \sum_i h_i \frac{dK_i}{dy} \tag{10}$$

or

$$\frac{dh}{dy} = C_{PR} \frac{dT}{dy} \tag{11}$$

where

$$C_{PR} = \left\{ C_{PM} + \sum_i h_i \frac{dK_i}{dT} \right\}$$

The energy equation becomes:

$$\rho v C_{PR} \frac{dT}{dy} = \frac{d}{dy}\left(\lambda \frac{dT}{dy}\right) + \mu\left(\frac{du}{dy}\right)^2 - \frac{d}{dy}\sum_i \rho_i V_i h_i \tag{12}$$

A simplification of the species continuity equations can be obtained through the introduction of the concept of "elemental" mass fractions as expressed by Lees in reference 6. The "elemental" mass fraction concept results from the fact that the mass of individual chemical elements is preserved in any chemical reaction not involving nuclear transformation. The "elemental" mass fraction is given by the expression:

$$\tilde{K}_j = \sum_i \zeta_{ij} \frac{M_j}{M_i} K_i$$

The species continuity equations for the elements can be obtained by multiplying equations (8) by $\zeta_{ij} M_j/M_i$ and summing over i, and there results the "elemental" species equations

$$\rho v \frac{d\tilde{K}_j}{dy} + \frac{d}{dy}\left(\sum_i \zeta_{ij} \frac{M_j}{M_i} \rho_i V_i\right) = 0 \qquad (13)$$

The introduction of the "elemental" mass fraction eliminates the species production terms (ω_i) of equations (8) and reduces the number of calculations to be made. There is now one equation of the above form for each element as opposed to one equation of the form of equation (8) for each chemical species.

In the present analysis there will be three elements H, N, and O, and four chemical species O_2, H_2, N_2, and H_2O considered with one chemical reaction of the form:

$$H_2 + \frac{1}{2} O_2 \leftrightarrows H_2O$$

This same chemical system was used by Libby and Pierucci in reference 1, and while it does not consider dissociation or ionization, the species considered do represent the major products of hydrogen combustion in an airstream. Also, the species considered have the necessary variation in molecular weight which is essential to the diffusion model comparisons.

Boundary Conditions

At the moving surface, (y = s), the following boundary conditions apply:

$$T = T_\infty$$

$$u = u_\infty$$

$$\tilde{K}_i = \tilde{K}_{i_\infty}$$

In order to simulate the two-dimensional boundary layer the "elemental" mass fraction for hydrogen must be very small. This creates a correspondingly small "elemental" hydrogen density and since the continuity equation must be satisfied (ρv = constant) the transverse velocity becomes very large. This introduces some uncertainty as the transverse velocity was assumed small in comparison with the main flow velocity in order to accomplish the reduction of the general equations of motion. This apparent contradiction is inherent in the use of the one-dimensional Couette flow to simulate the two-dimensional laminar boundary layer and arises primarily from the assumption of the porous surfaces being permeable only to the hydrogen.

At the lower surface, (y = 0), the boundary conditions are:

$$u = 0$$

$$T = T_w$$

The boundary conditions on the "elemental" species continuity equations are derived as follows. Integration of the global continuity equation yields

$$\rho v = \text{constant} = (\rho v)_w \tag{14}$$

Using this relation the "elemental" species continuity equation can be integrated to give:

$$\rho v\, K_j + \sum_i \zeta_{ij} \frac{M_j}{M_i} \rho_i V_i = \text{constant} \tag{15}$$

The following subscript notation is adopted for the "elemental" species.

element	subscript
O	1
H	2
N	4

Assuming Fick's law diffusion for illustration the diffusion velocities are

$$\rho_i V_i = - \rho D \frac{dK_i}{dy} \tag{15a}$$

and assuming the same relation holds for the "elemental" species

$$\tilde{\rho}_i \tilde{V}_i = - \rho D \frac{d\tilde{K}_i}{dy} \tag{15b}$$

Using the Fick's law relation, equation (15a), the summation term of equation (15) becomes,

$$\sum_i \zeta_{ij} \frac{M_j}{M_i} \rho_i V_i = - \rho D \sum_i{}' \zeta_{ij} \frac{M_j}{M_i} \frac{dK_i}{dy} \tag{15c}$$

The definition of the "elemental" mass fraction is

$$\tilde{K}_j = \sum_i \zeta_{ij} \frac{M_j}{M_i} K_i \tag{15d}$$

Differentiating equation (15d) one obtains,

$$\frac{dK_j}{dy} = \sum_i \zeta_{ij} \frac{M_j}{M_i} \frac{dK_i}{dy} \tag{15e}$$

Substituting equation (15e) into equation (15c) the following relationship is obtained,

$$\sum_i \zeta_{ij} \frac{M_j}{M_i} \rho_i V_i = - \rho D \frac{d\tilde{K}_j}{dy}$$

or from equation (15b),

$$\sum_i \zeta_{ij} \frac{M_j}{M_i} \rho_i V_i = \tilde{\rho}_j \tilde{V}_j$$

Thus equation (15) becomes

$$\rho v \tilde{K}_j + \tilde{\rho}_j \tilde{V}_j = \text{constant} \tag{15f}$$

Considering first the injected species, hydrogen, equation (15f) becomes:

$$\tilde{\rho}_2 v + \tilde{\rho}_2 \tilde{V}_2 = \text{constant}$$

$$\tilde{\rho}_2 (v + \tilde{V}_2) = \text{constant}$$

$$\tilde{\rho}_2 \tilde{v}_2 = \text{constant} \tag{16}$$

Evaluating the constant at the lower wall (y = 0) the above equation becomes:

$$\tilde{\rho}_2 \tilde{v}_2 = (\tilde{\rho}_2 \tilde{v}_2)_w = (\rho v)_w$$

Thus the boundary condition on the "elemental" hydrogen continuity equation becomes:

$$(\rho v)_w \tilde{K}_{2w} + \sum_i \zeta_{ij} \frac{M_j}{M_i} \rho_i V_{i_w} = (\rho v)_w$$

or

$$\tilde{K}_{2w} = 1 - \frac{1}{(\rho v)_w} \left(\sum \frac{\zeta_{ij} M_j}{M_i} \rho_i V_i \right)_w \tag{17}$$

A similar procedure is followed in evaluating the constant for the main stream components where

$$\tilde{\rho}_1 \tilde{v}_1 = (\tilde{\rho}_1 \tilde{v}_1)_w = 0$$

$$\tilde{\rho}_4 \tilde{v}_4 = (\tilde{\rho}_4 \tilde{v}_4)_w = 0$$

The boundary conditions for these elements

$$\tilde{K}_{1w} = - \frac{1}{(\rho v)_w} \left(\sum_i \zeta_{ij} \frac{M_j}{M_i} \rho_i V_i \right)_w \tag{18}$$

$$\tilde{K}_{4w} = - \frac{1}{(\rho v)_w} \left(\sum_i \zeta_{ij} \frac{M_j}{M_i} \rho_i V_i \right)_w \tag{19}$$

Nondimensional Form of the Governing Equations

The following new variables are introduced:

$$\eta = \frac{y}{s} \qquad U = \frac{u}{u_\infty}$$

$$\theta = \frac{T}{T_\infty} \qquad \delta_o = \frac{\rho v s}{\mu_\infty} = \frac{(\rho v)_w s}{\mu_\infty}$$

The governing equations in nondimensional form are:

momentum equation,

$$\delta_o \frac{dU}{d\eta} = \frac{d}{d\eta} \left(\frac{\mu}{\mu_\infty} \frac{dU}{d\eta} \right) \tag{20}$$

energy equation,

$$\delta_o \frac{C_{PR}}{C_{PR_\infty}} \frac{d\theta}{d\eta} = \frac{d}{d\eta} \left(\frac{\lambda}{C_{PR_\infty} \mu_\infty} \frac{d\theta}{d\eta} \right) + \frac{u_\infty^2 \mu}{C_{PR_\infty} T_\infty \mu_\infty} \left(\frac{dU}{d\eta} \right)^2$$

$$- \frac{d}{d\eta} \left(\sum_i \frac{\rho_i V_i s}{\mu_\infty} \frac{h_i}{C_{PR_\infty} T_\infty} \right) \tag{21}$$

species continuity equation,

$$\delta_o \frac{d\tilde{K}_j}{d\eta} = - \frac{d}{d\eta}\left(\sum_i \zeta_{ij} \frac{M_j}{M_i} \frac{\rho_i V_i s}{\mu_\infty}\right) \tag{22}$$

Nondimensional Boundary Conditions

At $\eta = 1$

$$U = 1$$

$$\theta = 1$$

$$\tilde{K}_i = \tilde{K}_{i_\infty}$$

at $\eta = 0$

$$U = 0$$

$$\theta = \theta_w$$

$$\tilde{K}_{2w} = 1 - \frac{1}{\delta_o}\left(\sum_i \zeta_{ij} \frac{M_j}{M_i} \frac{\rho_i V_i s}{\mu_\infty}\right)_w \tag{23}$$

$$\tilde{K}_{1w} = - \frac{1}{\delta_o}\left(\sum_i \zeta_{ij} \frac{M_j}{M_i} \frac{\rho_i V_i s}{\mu_\infty}\right)_w \tag{24}$$

$$\tilde{K}_{4w} = - \frac{1}{\delta_o}\left(\sum_i{}' \zeta_{ij} \frac{M_j}{M_i} \frac{\rho_i V_i s}{\mu_\infty}\right)_w \tag{25}$$

Heat Transfer at Lower Wall

$$Q_w = \lambda \frac{dT}{dy}\Big)_w - \sum_i \rho_i V_i h_i\Big)_w \tag{26}$$

Transforming equation (26),

$$q_w = \frac{Q_w s}{\mu_\infty C_{PR_\infty} T_\infty} = \frac{\lambda}{\mu_\infty C_{PR_\infty}} \frac{d\theta}{d\eta}\Bigg)_w - \sum_i \frac{\rho_i V_i s}{\mu_\infty} \frac{h_i}{C_{PR_\infty} T_\infty}\Bigg)_w \tag{26a}$$

Shear Stress at Lower Wall

$$\tau_w = \mu_w \frac{du}{dy}\Bigg)_w \tag{27}$$

Transforming equation (27),

$$C_f = \frac{\tau_w s}{\mu_\infty \mu_\infty} = \frac{\mu_w}{\mu_\infty} \frac{dU}{d\eta}\Bigg)_w \tag{27a}$$

Solid Wall Couette Flow

For the solid wall case, the mass transfer is zero. The continuity equation integrates to:

$$\rho v = 0 \tag{28}$$

The governing equations then reduce to:

momentum equation,

$$\frac{d}{dy}\left(\mu \frac{du}{dy}\right) = 0 \tag{29}$$

energy equation,

$$\frac{d}{dy}\left(\lambda \frac{dT}{dy}\right) + \mu\left(\frac{du}{dy}\right)^2 = 0 \tag{30}$$

On introduction of the nondimensional variables these equations become:

momentum equation,

$$\frac{d}{d\eta}\left(\mu \frac{dU}{d\eta}\right) = 0 \tag{31}$$

energy equation,

$$\frac{d}{d\eta}\left(\lambda T_\infty \frac{d\theta}{d\eta}\right) + \mu u_\infty^2\left(\frac{dU}{d\eta}\right)^2 = 0 \tag{32}$$

Integrating each equation once and evaluating the constant at the lower surface the equations in nondimensional form are:

momentum equation,

$$\frac{dU}{d\eta} = \frac{C_1}{\mu} \tag{33}$$

where

$$C_1 = \mu_w \frac{dU}{d\eta}\Bigg)_w$$

energy equation,

$$\frac{d\theta}{d\eta}\Bigg) = -\frac{1}{\lambda(\eta)} \int_0^\eta \frac{\mu(\eta) u_\infty}{T_\infty}\left(\frac{dU}{d\eta}\right) d\eta + \frac{C_2}{\lambda(\eta)} \tag{34}$$

where

$$C_2 = \lambda_w \left.\frac{d\theta}{d\eta}\right)_w$$

Boundary Conditions

$\eta = 1$

$$U = 1$$

$$\theta = 1$$

$\eta = 0$

$$U = 0$$

$$\theta = \theta_w$$

Heat Transfer at Lower Wall

$$Q_w = \lambda_w \left.\frac{dT}{dy}\right)_w \tag{35}$$

Transforming,

$$q_{w_o} = \frac{Q_w s}{\mu_\infty C_{PR_\infty} T_\infty} = \frac{\lambda_w}{C_{PR_\infty \mu_\infty}} \left.\frac{d\theta}{d\eta}\right)_w \tag{35a}$$

Shear Stress at Lower Wall

$$\tau_w = \mu_w \left.\frac{du}{dy}\right)_w \tag{36}$$

Transforming,

$$C_{f_o} = \frac{\tau_w s}{\mu_\infty \mu_\infty} = \frac{\mu_w}{\mu_\infty} \frac{dU}{d\eta}\Bigg)_w \qquad (36a)$$

IV. GAS PROPERTIES

The thermodynamic and transport properties are calculated by the methods listed below. The gas mixture is assumed to be at one atmosphere pressure for all calculations.

Chemical Composition

The following reaction is considered for the present analysis:

$$H_2 + \frac{1}{2} O_2 \rightleftarrows H_2O$$

In addition, N_2 is present in the main Couette flow giving a total of four chemical species to be considered in the equilibrium calculations. The chemical equilibrium equations will be formulated in terms of the "elemental" mass fractions to facilitate calculation of the equilibrium composition from the solutions of the species continuity equations.

$$\tilde{K}_j = \frac{M_j}{\bar{M}} \sum_i \zeta_{ij} X_i \tag{37}$$

$$\tilde{K}_O = \frac{M_O}{\bar{M}} \left\{ 2X_{O_2} + X_{H_2O} \right\} \tag{38}$$

$$\tilde{K}_H = \frac{M_H}{\bar{M}} \left\{ 2X_{H_2} + 2X_{H_2O} \right\} \tag{39}$$

$$\tilde{K}_N = \frac{M_N}{\bar{M}} \left\{ 2X_{N_2} \right\} \tag{40}$$

Dividing equation (40) into equation (38) and rearranging one obtains the following equation for the mole fraction of N_2:

$$X_{N_2} = \frac{X_{O_2}}{A} + \frac{X_{H_2O}}{2A} \tag{41}$$

where:

$$A = \frac{M_N}{M_O} \frac{\tilde{K}_O}{\tilde{K}_N}$$

Dividing equation (40) into equation (39) and rearranging one obtains:

$$BX_{N_2} = X_{H_2} + X_{H_2O} \tag{42}$$

where:

$$B = \frac{M_N}{M_H} \frac{\tilde{K}_H}{\tilde{K}_N}$$

Substituting equation (41) into equation (42) the equation for the mole fraction of H_2 is obtained:

$$X_{H_2} = X_{H_2O}\left(\frac{C}{2} - 1\right) + CX_{O_2} \tag{43}$$

where:

$$C = \frac{B}{A}$$

Using the relation $\sum_i X_i = 1$,

$$X_{O_2} + X_{N_2} + X_{H_2O} + X_{H_2} = 1 \tag{44}$$

Substituting equations (43) and (41) into equation (44) the following relationship results:

$$\left\{1 + C + \frac{1}{A}\right\} X_{O_2} + \left\{\frac{C}{2} + \frac{1}{2A}\right\} X_{H_2O} = 1 \tag{45}$$

Letting

$$E = \left\{1 + C + \frac{1}{A}\right\}$$

$$F = \left\{\frac{C}{2} + \frac{1}{2A}\right\}$$

$$G = \frac{1}{F}$$

$$X_{H_2O} = (G - EGX_{O_2}) \tag{46}$$

Combining equation (46) and (43) one obtains:

$$X_{H_2} = \left\{\frac{C}{2} - 1\right\} (G - EGX_{O_2}) + CX_{O_2} \tag{47}$$

The equilibrium constant is related to the mole fractions by

$$P^{1/2}K_p = \frac{X_{H_2O}}{X_{H_2}(X_{O_2})^{1/2}} \tag{48}$$

Substituting equations (46) and (47) into equation (48) there results the following relation:

$$P^{1/2}K_p = \frac{(G - EGX_{O_2})}{\left\{\left(\frac{C}{2} - 1\right)(G - EGX_{O_2}) + CX_{O_2}\right\}(X_{O_2}{}^{1/2})}$$

Letting

$$I = P^{1/2}K_p$$

$$H = \frac{C}{2} - 1$$

the above relation reduces to

$$I = \frac{(G - EGX_{O_2})}{(HG - HEGX_{O_2} + CX_{O_2})(X_{O_2}{}^{1/2})}$$

$$IHGX_{O_2}{}^{1/2} - IHEGX_{O_2}{}^{3/2} + ICX_{O_2}{}^{3/2} = G - EGX_{O_2}$$

$$\left(\frac{C}{H} - EG\right)X_{O_2}{}^{3/2} + \frac{EG}{IH}X_{O_2} + GX_{O_2}{}^{1/2} = \frac{G}{IH} \qquad (49)$$

Since all the constants (A through I) in equation (49) are known quantities, equation (49) can be solved iteratively for the unknown mole fraction X_{O_2}. With the mole fraction X_{O_2} the other mole fractions can be easily determined from equations (46), (43), and (41). The equilibrium

constant used in these calculations is taken from the JANAF tables, reference 7, where it is tabulated in one hundred degree Kelvin increments.

The molecular weight of the mixture is determined from:

$$\bar{M} = \sum_i X_i M_i \tag{50}$$

The mass fractions are determined from the mole fractions by:

$$K_i = \frac{X_i M_i}{\bar{M}} \tag{51}$$

Thermodynamic Properties

The mixture density is obtained from the perfect gas law

$$\rho = \frac{P\bar{M}}{RT} \tag{52}$$

and the enthalpy of the individual species is taken from the JANAF tables, reference 7, and the mixture enthalpy is calculated by

$$h_m = \sum_i K_i h_i \tag{53}$$

where

$$h_i = \int_{T^o}^{T} C_{P_i}\, dT + h^o_{f_i} \text{ (ref. 7)}$$

The reference temperature for the present calculations is 0^o K.

The specific heat of the individual species is also taken from reference 7. The specific heat of the mixture is obtained from the relation

$$C_{PR} = \sum_i K_i C_{Pi} + \sum_i h_i \frac{dK_i}{dT} \tag{54}$$

The derivative of K_i is found numerically by solving for the K_i's at a temperature 25° K above and below the given temperature with:

$$\frac{dK_i}{dT} = \frac{K_i^{(T+25)} - K_i^{(T-25)}}{50} \tag{55}$$

A comparison of the present method and the method of Zeleznik and Gordon, reference 8, is given in table I which shows very good agreement between the two methods.

Transport Properties

Rigorous kinetic theory expressions for the viscosity and thermal conductivity of gas mixtures have been developed and are presented by Hirschfelder et al. in reference 9, but these expressions are mathematically cumbersome. Somewhat simpler relations, which are approximations derived from the rigouous expressions are given by Brokaw in reference 10 and are used in the present analysis. These approximations are very accurate at low temperatures but the accuracy is expected to deteriorate somewhat at higher temperatures due to uncertainties in the approximations and molecular constants used, however, these approximations are of sufficient accuracy for use in the expected temperature range of the present analysis.

Mixture Viscosity

The mixture viscosity is calculated from the pure component viscosities with the relation

$$\mu_M = \sum_i \frac{\mu_i}{1 + \sum_{\substack{j=1 \\ j \neq i}} \Phi_{ij} \frac{X_j}{X_i}} \tag{56}$$

The coefficients Φ_{ij} are a function of the pure component viscosities and molecular weight ratios

$$\Phi_{ij} = \frac{\left[1 + \left(\frac{\mu_i}{\mu_j}\right)^{1/2} \left(\frac{M_j}{M_i}\right)^{1/4}\right]^2}{2\sqrt{2}\left(1 + \left(\frac{M_i}{M_j}\right)\right)^{1/2}} \tag{57}$$

For use in the present analysis the pure component viscosities are taken from Svehla, reference 11.

Mixture Thermal Conductivity

The mixture thermal conductivity is obtained from the relation:

$$\lambda_m = \lambda_m' + \lambda_m'' \tag{58}$$

where λ_m' is the transfer of energy due to the translational motion of the molecules and λ_m'' is the transfer of energy between internal degrees of freedom and translational motion in polyatomic molecules. The

monatonic mixture conductivity is obtained from the pure component monatonic conductivities with the relation

$$\lambda'_m = \sum_i \frac{\lambda'_i}{1 + \sum_{\substack{j=1 \\ j \neq i}} \psi_{ij} \frac{X_j}{X_i}} \tag{59}$$

The coefficient ψ_{ij} is obtained from the viscosity coefficient Φ_{ij} by following relationship

$$\psi_{ij} = \Phi_{ij} \left\{ 1 + 2.41 \left[\frac{(M_i - M_j)(M_i - 0.142\, M_j)}{(M_i + M_j)^2} \right] \right\} \tag{60}$$

The internal mixture conductivity is obtained from the pure component internal conductivities with the relation

$$\lambda''_m = \sum_i \frac{\lambda''_i}{1 + \sum_{\substack{j=1 \\ j \neq i}} \Phi_{ij} \frac{X_j}{X_i}} \tag{61}$$

The pure component thermal conductivities are obtained from reference 11.

The pure component transport properties used in the analysis are calculated in reference 11 by:

Viscosity

$$\mu = \frac{26.693 \sqrt{MT}}{\sigma^2 \Omega(2,2)^*} \times 10^{-6} \tag{62}$$

Monatonic Thermal Conductivity

$$\lambda' = \frac{15R}{4M}\mu \tag{63}$$

Internal Thermal Conductivity

$$\lambda'' = 1.32\,\frac{R}{M}\left(\frac{C_P}{R} - \frac{5}{2}\right)\mu \tag{64}$$

In calculating the viscosities and thermal conductivities using the above equations the Lennard-Jones (12-6) potential was used to obtain the reduced collision integrals $\Omega(2,2)^*$. The reduced collision integrals are given in table form in reference 9. The molecular force constants (see table II) used in the Lennard-Jones (12-6) potential were obtained from experimental viscosity and thermal conductivities where possible and estimated by Svehla in reference 11 using empirical relations where no data was available. In the calculation of the reduced collision integral the molecules were all assumed to be nonpolar. This assumption does not introduce appreciable error since the force constants were obtained from viscosity measurements and since the dipole-dipole interaction is negligible in higher temperature high energy collisions. A more complete discussion can be found in reference 11.

Diffusion Transport

The purpose of the present analysis is to compare solutions to the governing equations for Couette flow using two different diffusion models; the approximate Fick's law diffusion model and the more exact multicomponent

diffusion model. As will be seen below, the more exact multicomponent diffusion model entails a considerable number of mathematical operations and from a numerical analysis standpoint is not as desirable as the simpler but approximate Fick's law model. These two diffusion models are presented in the following sections.

Multicomponent Diffusion

The multicomponent diffusion fluxes were calculated using the following relations from reference 9.

$$\frac{dX_i}{dy} = \sum_{\substack{j=1 \\ j\neq i}}^{\nu-1} \frac{X_i X_j}{\mathcal{D}_{ij}}(V_j - V_i) \tag{65}$$

Equation (65) is the Stephan-Maxwell relationship for the multicomponent diffusion velocities.

$$\sum_{i=1}^{\nu} \rho_i V_i = 0 \tag{66}$$

Equation (65) can be rearranged to a more convenient form:

$$\frac{dX_i}{dy} = \sum_{\substack{j=1 \\ j\neq i}}^{\nu-1} \left(\frac{X_i X_j}{\mathcal{D}_{ij}} V_j \right) - V_i \sum_{\substack{j=1 \\ j\neq i}}^{\nu-1} \frac{X_i X_j}{\mathcal{D}_{ij}} \tag{67}$$

Multiplying equation (67) by ρ/μ_∞ and introducing the nondimensional coordinates we have:

$$\frac{\rho}{\mu_\infty} \frac{dX_i}{d\eta} = \sum_{\substack{j=1 \\ j\neq i}}^{\nu-1} \frac{X_i X_j}{K_j \mathcal{D}_{ij}} \frac{\rho_j V_j s}{\mu_\infty} - \frac{\rho_i V_i s}{\mu_\infty} \sum_{\substack{j=1 \\ j\neq i}}^{\nu-1} \frac{X_i X_j}{K_i \mathcal{D}_{ij}} \tag{68}$$

Similarly multiplying equation (66) by s/μ_∞:

$$\sum_{i=1}^{\nu} \frac{\rho_i V_i s}{\mu_\infty} = 0 \tag{69}$$

For the ν component gas mixture the diffusion fluxes, $\rho_i V_i s/\mu_\infty$, are obtained from the simultaneous solution of $\nu - 1$ relations of the form of equation (68) and the relation given by equation (69).

The binary diffusion coefficients are calculated using the following relation from reference 9.

$$\mathcal{D}_{ij} = 0.002628 \left[\frac{\left(\frac{T^3 (M_i + M_j)}{2 M_i M_j} \right)^{1/2}}{P(\sigma_{ij})^2 \, \Omega_{ij}^{(1,1)*}} \right] \tag{70}$$

Again the reduced collision integral, $\Omega_{ij}^{(1,1)*}$, is based on the Lennard-Jones potential and is taken from reference 9. The molecular constants used for these calculations and to obtain the reduced collision integrals are given in table II. The binary diffusion coefficients obtained from the above relation are shown in figure 2.

Fick's Law Diffusion

The Fick's law diffusion fluxes are calculated according to the following relation:

$$\rho_i V_i = - \rho D \frac{dK_i}{dy} \tag{71}$$

Knuth in reference 12 states that a sufficient condition for the applicability of equation (71) is that the binary diffusion coefficients are equal to each other and to the Fick's law diffusion coefficient. This assumption makes the Fick's law diffusion coefficient a pseudo binary diffusion coefficient and in the literature Fick's law diffusion is generally referred to as binary diffusion because of the appearance of equation (71). The term binary diffusion will be adopted here for discussion purposes.

Multiplying equation (71) by $1/\mu_\infty$ and introducing the nondimensional coordinates equation (71) becomes

$$\frac{\rho_i V_i s}{\mu_\infty} = - \frac{\rho D}{\mu_\infty} \frac{dK_i}{d\eta}$$

The diffusion coefficient is considered to be the same for all species and as such is a self-diffusion coefficient given by the following relation from reference 9:

$$D = 0.002628 \left[\frac{(T^3/\bar{M})^{1/2}}{P(\sigma_{ij})^2 \Omega_{ij}^{(1,1)*}} \right] \tag{72}$$

where the molecular constants are an average of those in table II. Again the Lennard-Jones collision integral is used. The mixture molecular weight is used in place of an average molecular weight in order to more accurately represent the diffusion process. Although not plotted on figure 2, the average diffusion coefficient lies above

the lower set of curves and below the upper set. Thus at a given temperature the average diffusion coefficient lies in a narrow band of values depending on the mixture molecular weight.

V. COMPUTATION

The philosophy on the numerical analysis was to keep calculations straightforward and as simple as possible. Some changes were made in the numerical technique during the debugging process but overall the numerical analysis is straightforward while not always simple.

Solid Wall Couette Flow

The governing equations for the solid wall Couette flow are arranged as follows:

momentum equation,

$$\frac{dU}{d\eta} = f_u(\eta) \tag{73}$$

where

$$f_u(\eta) = \frac{C_1}{\mu(\eta)}$$

energy equation,

$$\frac{d\theta}{d\eta} = f_\theta(\eta) \tag{74}$$

where

$$f_\theta(\eta) = -\frac{1}{\lambda(\eta)}\int_0^\eta \mu(\eta)\,\frac{u_\infty^2}{T}\left(\frac{dU}{d\eta}\right)^2 d\eta + \frac{C_2}{\lambda(\eta)}$$

The solution of each individual equation is obtained using the "corrector" method given by Hamming in reference 13. This method is based on an iterative finite-difference procedure using the following equation:

$$F_{N+1} = F_N + \frac{\Delta\eta}{2}\left\{F'_{N+1} + F'_N\right\} \tag{75}$$

where $\Delta\eta$ is the distance between finite-difference stations. According to references 13 and 14 the iterated corrector process always converges. In the evaluation of the $f_u(\eta)$ and $f_\theta(\eta)$ it is necessary to obtain derivatives of several functions and this numerical differentiation is accomplished through the use of the equations given in appendix A. Initial starting profiles are obtained from constant property solutions to the governing equations for Couette flow. Then solutions to the energy and momentum equations are obtained by repeated (iterated) application of the corrector equation until the following error criterion is met:

$$\left| F_N^{I+1} - F_N^{I} \right| \leq 0.000001$$

That is, the right-hand sides of equations (73) and (74) are evaluated at each finite-difference station and the resulting functions integrated using equation (75). This process is repeated until the above error criterion is met. The simultaneous solution of the energy and momentum equations is accomplished by the iteration technique of Smith and Clutter,

reference 15. This iteration process is shown in figure 3 and the block labeled "Fluid Properties" is simply the determination of the transport properties. The simultaneous solution is assumed to converge when the momentum equation has satisfied the following error criterion:

$$\left| U_N^{I+1} - U_N^{I} \right| \leq 0.000001$$

The present method for the solid wall Couette flow has been compared to several calculations from the literature. Air Couette flow comparisons have been made with the constant property analytical method of Eckert and Schneider, reference 2, for the following conditions:

$$T_\infty = 218^\circ \text{ K}$$

$$\text{Mach No.} = 12$$

$$\theta_w = 6$$

Only the temperature profile is compared as the velocity profile is linear in both methods. Good agreement was obtained between the two methods as shown in figure 4. In the constant property solutions the terms "edge" and "wall" refer to the moving and stationary surfaces, respectively, where the values of the properties were fixed for the solutions. Also present in figure 4 for general interest is the variable property solution and it is seen that the constant property solutions do not represent the variable property solution to any great degree.

A variable property solution for nitrogen Couette flow was taken from reference 3 and is compared to the present method for a nitrogen stream in figure 5, with good agreement again being obtained. The

velocity profile (not shown) also showed good agreement. This comparison was made for the following conditions:

$$T_\infty = 218^\circ \text{ K}$$

$$\text{Mach No.} = 12$$

$$T_w = 872^\circ \text{ K}$$

The nondimensional coordinate γ is given by

$$\gamma = \frac{\alpha}{\alpha_\delta}$$

where

$$\alpha_\delta = \int_0^1 \frac{d\eta}{\mu}$$

and the nondimensional temperature θ_1 is given by

$$\theta_1 = \frac{T - T_w}{T_\infty - T_w}$$

Couette Flow With Injection

The governing equations for Couette flow with hydrogen injection are arranged as follows:

momentum equation,

$$\frac{dU}{d\eta} = f_u(\eta) \tag{76}$$

where

$$f_u(\eta) = \frac{1}{\delta_o} \frac{d}{d\eta}\left(\frac{u}{\mu_\infty} \frac{dU}{d\eta}\right) \tag{77}$$

energy equation,

$$\frac{d\theta}{d\eta} = f_\theta(\eta) \tag{78}$$

where

$$f_\theta(\eta) = \frac{C_{PR_\infty}}{\delta_o C_{PR}}\left\{\frac{d}{d\eta}\left(\frac{\lambda}{\mu_\infty C_{PR_\infty}} \frac{d\theta}{d\eta}\right)\right.$$

$$\left. + \frac{u_\infty \mu}{C_{PR_\infty} T_\infty \mu_\infty}\left(\frac{dU}{d\eta}\right)^2 - \frac{d}{d\eta} \sum_i \left(\frac{\rho_i V_i s}{\mu_\infty} \frac{h_i}{T_\infty C_{PR_\infty}}\right)\right\} \tag{79}$$

species continuity equation

$$\delta_o \frac{d\tilde{K}_i}{d\eta} = - \frac{d}{d\eta} \sum_i \frac{\zeta_{ij} M_j}{M_i} \frac{\rho_i V_i s}{\mu_\infty} \tag{80}$$

The "elemental" species continuity equation can be integrated to provide a more easily applied form so that the "elemental" mass fractions can be directly determined.

Integrating:

$$\delta_o \tilde{K}_j = - \sum_i \frac{\zeta_{ij} M_j}{M_i} \frac{\rho_i V_i s}{\mu_\infty} + \text{constant}$$

Evaluating the constant for the main stream components at $\eta = 0$

for nitrogen

$$\text{constant} = (\tilde{\rho}_4 \tilde{v}_4)_w = 0$$

for oxygen

$$\text{constant} = (\tilde{\rho}_1 \tilde{v}_1)_w = 0$$

The constant of zero for both "elements" results directly from the boundary conditions, equations (24) and (25).

Thus the species continuity equation for the main stream components becomes:

$$\tilde{K}_j = - \frac{1}{\delta_o} \left(\sum_i \frac{\zeta_{ij} M_j}{M_i} \frac{\rho_i V_i s}{\mu_\infty} \right) \tag{81}$$

Since there are three "elements" in the system only two species continuity equations need be solved, for the sum of the "elemental" mass fractions equal one.

Because some difficulty was encountered in the solution of the governing equations, the presentation of the numerical analysis will be somewhat in a reverse order from that of the solid wall case. However, the initial starting profiles are again obtained from the constant property solutions to the governing equations for Couette flow.

The simultaneous solution of the governing equations is again accomplished by the iteration technique of Smith and Clutter, reference 15, but with one minor change. The iteration process is shown in figure 3 and the block labeled "Fluid Properties" is expanded in figure 6. The "Fluid Properties" loop is necessary because the iterative solution of the "elemental" species continuity equations requires a new calculation of the chemical composition and diffusion velocities after each iteration. The "elemental" species continuity equations are assumed to be satisfied when the boundary conditions meet the following criterion:

$$\frac{\tilde{K}_{i_{CAL}}^{J} - \tilde{K}_{i_{B.C.}}^{J}}{\tilde{K}_{i_{B.C.}}^{J}} \leq 0.002$$

The choice of 0.2 percent as the error criterion was dictated by the economics of computer usage for it was found that the major iteration (time-consuming calculations) were those in the "Fluid Properties" loop. The overall simultaneous solution of the governing equations was said to have been obtained when the following error criterion on the momentum equation was met:

$$\frac{U_N{}^{I+1} - U_N{}^{I}}{U_N{}^{I+1}} \leq 0.001$$

The error criterion of 0.1 percent was again dictated by the computer time used to obtain a solution. Within the major loops of the iteration process in figure 2 the energy equation was assumed converged when:

$$\frac{\theta_N{}^{I+1} - \theta_N{}^{I}}{\theta_N{}^{I+1}} \leq 0.001$$

and again the error criterion was 0.1 percent.

Initially the solution of the energy, momentum, and species continuity equations was attempted using the "corrector" equation given previously and the three-point derivative formulas. However, when the simultaneous solution converged there were present large oscillations in the solution, especially in the temperature (θ) profile. An attempt to alleviate the problem was made by attempting to use a more accurate derivative formula, such as the five-point formula given below from reference 16.

$$\left.\frac{dF}{d\eta}\right)_N = \frac{- F_{N+2} + 8F_{N+1} - 8F_{N-1} + F_{N-2}}{12\Delta\eta} \tag{82}$$

where the error term was of order $(\Delta\eta)^4$. The oscillations became worse. Although the above formula is more accurate than the three-point formulas of appendix A both formulas have the same feature; they do not include the value at the point of calculation. In place of the three- and five-point formulas a four-point formula was derived, see appendix B, which considerably reduced the oscillations but did not completely eliminate them. The "corrector" formula, equation (75), is but a two-point (trapezoidal) integration relation and in the region of rapid changes in the function to be integrated it is not very accurate. However, reference 17 gives some six-point integration formulas that are more

accurate and these formulas, see appendix C, are used for the present calculations resulting in a smoothing out of the oscillations in the converged solution.

The solution to the individual momentum and energy equations was obtained by iterating the six-point integration formulas until the following error criterion was met:

$$\left|F_N{}^{J+1} - F_N{}^{J}\right| \leq 0.000001$$

That is, the right-hand sides of equations (76) and (78) are evaluated at each finite-difference station and the resulting functions then integrated using the six-point formulas of appendix C to obtain the velocity (U) and temperature (θ) profiles. This procedure is repeated until the velocity and temperature profiles meet the above error criterion.

The present method for Couette flow with hydrogen injection has been compared with the solutions of Simon et al., reference 3, for the following conditions:

$$T_\infty = 218^\circ \text{ K}$$

$$\text{Mach No.} = 12$$

$$T_w = 872^\circ \text{ K}$$

$$Re_v = 0.5$$

where:

$$Re_v = \rho v s \int_0^\eta \frac{1}{\mu}\, d\eta$$

The stream is all nitrogen and has variable properties and binary diffusion. In general very good agreement between the methods was obtained. Figure 7 shows the temperature profile comparisons with the agreement not as good as expected but within reason. Better agreement was obtained between the velocity and concentration profiles as shown in figure 8. On the basis of the comparison made here it is assumed that the numerical technique is sufficiently accurate to carry out the present investigation.

VI. DISCUSSION OF RESULTS

The following values of the independent variables were used to obtain both binary (Fick's law) and multicomponent diffusion solutions:

$$\left.\begin{aligned} T_\infty &= 218^\circ \text{ K} \\ \text{Mach No.} &= 6 \\ T_w &= 872^\circ \text{ K} \end{aligned}\right\} \text{For all cases}$$

and δ_o = 0., 0.05, 0.1, 0.13, 0.2, 0.35, 0.5, 0.75, 1., 1.3.

In the numerical calculations fifty finite-difference stations were used for all cases except the no injection case where forty stations were used. The solutions were obtained on a CDC 6600 computer and run times for a single case varied from a few seconds for the no injection solution to about thirty minutes for the multicomponent diffusion solutions at large injection rates. The convergence of the total solution was fairly rapid, requiring generally about four iterations of the momentum equation. Referring to figure 3, each iteration of the momentum equation required fewer iterations of the energy equation, with the total number of energy equation iterations being about five times the total number of momentum equation iterations. By far the most iterations were made in the "Fluid Properties" loop of figure 6 with a total number of iterations varying from several hundred to several thousand depending on the initial starting profiles and the magnitude of the injection rate. The numerical technique of this thesis is not very sophisticated in terms of present day numerical analysis but there has not been a single case of nonconvergence encountered with this technique.

The no injection temperature and velocity profiles are given in figure 9 and it should be noted that the stream temperature increases only slightly above the wall value, indicating that for the present conditions the wall temperature is less than but close to the adiabatic wall temperature. The velocity profile is not a linear profile due to the viscosity variation through the stream.

Velocity Profiles

The nondimensional velocity profiles are given in figures 10 through 14. There does not appear to be any major difference between the solutions for the binary and multicomponent diffusion models, especially at the lower injection rates where the amount of hydrogen and water are substantially reduced in comparison to the oxygen and nitrogen. Also, the binary and multicomponent diffusion model velocity profiles in the region of the lower wall do not show any significant differences and in most cases the differences are hardly detectable. However, there is a difference in the nondimensional shear stress at the lower wall as shown in figure 15. The shear stress for the multicomponent diffusion model is higher than the corresponding binary diffusion model solutions for all injection rates. This shear stress difference results primarily from the mixture viscosity variations between the two diffusion models. The pure component viscosities for hydrogen and water are lower than those for nitrogen and oxygen, resulting in decreasing mixture viscosity with increasing hydrogen and water concentrations. As will be shown in the section on concentration profiles, the hydrogen and water concentrations at the lower wall for

the binary diffusion model are greater than the corresponding multicomponent diffusion model solutions, hence, the mixture viscosity is less at the wall in the binary diffusion solutions. This decreased viscosity causes the somewhat reduced shear stress for the binary diffusion model as seen in figure 15.

In the present solutions the shear stress for both diffusion models increases substantially over the no injection condition in the intermediate injection rate range. This effect was not seen in the results of Eckert and Schneider, reference 2, where the shear stress was shown to decrease from the no injection condition for all hydrogen injection rates. Since reference 2 did not consider variable properties nor chemical reactions the increased shear stress of the present calculations is attributed to the inclusion of these phenomena in the analysis.

Temperature Profiles

The nondimensional temperature profiles are given in figures 16 through 20. The differences between the binary and multicomponent diffusion models are greater for the temperature profiles than was the case for the velocity profiles with these differences being greatest at the intermediate hydrogen injection rates. The overwhelming effect of chemical reaction is seen by comparing the no injection temperature profile of figure 9 with figures 16 through 20. The increase in peak stream temperature over the no injection solution approaches a factor of three at the higher injection rates. Referring to figure 21 it is apparent that at low and intermediate injection rates the lower wall heating substantially increases but the heating rate then decreases as

the injection rate is increased further. These heating rate curves point out one of the largest differences between the diffusion model assumptions. The heating rates for the binary diffusion model are always larger than the corresponding multicomponent diffusion model and are positive, whereas the multicomponent diffusion model lower wall heating rate is negative at the largest injection rate.

The no chemical reaction results of Eckert and Schneider, reference 2, do not show the large temperature and heating rate increases that result when the exothermic hydrogen oxygen reaction is considered. Aside from this large effect of chemical reaction on the temperature profiles, the differences between the two diffusion models is more apparent especially in the heat transfer rates where the binary diffusion model generally predicts much larger heating rates than the multicomponent diffusion model.

Concentration Profiles

The differences between the two diffusion models is best seen in the concentration profiles of figures 22 through 30, where not only are there differences in the relative amounts of species but there are also some profile shape variations. The biggest difference occurs in the hydrogen concentration profile with the wall concentration reflecting this difference the most. Figure 31 gives the hydrogen concentration at the wall for both diffusion models and it is readily seen that the binary diffusion model concentration is much larger than the corresponding multicomponent model. This large difference alters the mixture transport properties at the wall, for hydrogen has a larger thermal conductivity

and lower viscosity than the other species. This alteration of transport properties is the primary cause of the heating rate differences of figure 21, for the temperature profiles of the two diffusion models are very close at the wall whereas the heating rate due to conduction alone is less for the multicomponent model due to the lower hydrogen concentration.

The differences between the concentration profiles for the two diffusion models is primarily due to the increased diffusion velocities of the multicomponent model which means that a smaller chemical species gradient is needed to produce the same diffusion velocity as the binary model. This lowers the hydrogen concentration at the wall and also causes the reaction zone to be at a greater distance from the lower wall. This is best seen in figure 29 for an injection rate $\delta_o = 0.1$ where for the binary diffusion model the reaction zone is away from the surface.

The concentration profiles point out the area of greatest difference between the two diffusion models, with the concentration of hydrogen at the lower wall best representing these differences.

VII. CONCLUSIONS

The foregoing analysis has resulted in the following conclusions:

1. Hydrogen injection into air Couette flow with chemical reaction alters the stream properties and causes changes in the major flow variables.

2. There are significant differences between the two diffusion models, and the approximate Fick's law diffusion model should be avoided except where gross approximations to the flow variables are needed.

3. The injection of hydrogen into air Couette flow with chemical reactions generally results in an increase in skin friction and heating rate.

4. Major differences between the two diffusion models is manifested in the concentration profiles where not only are the concentrations different but there is some variation in profile shapes.

5. The multicomponent diffusion model solutions for the lower wall shear stress show an increase in the shear stress over the corresponding Fick's law diffusion solutions.

6. The multicomponent diffusion model solutions for the lower wall heating rates generally show a decrease in heating rate over the corresponding Fick's law diffusion solutions.

VIII. RECOMMENDATION

It is recommended that a study similar to this one be carried out for the two-dimensional laminar boundary layer to establish the validity of using Couette flow with hydrogen injection and chemical reactions to simulate a chemically reacting two-dimensional laminar boundary layer with hydrogen injection.

REFERENCES

1. Libby, P. A.; Pierucci, M.: Laminar Boundary Layer With Hydrogen Injection Including Multicomponent Diffusion, AIAA Journal, Vol. 2, No. 12, December 1964, pp. 2118-2126.

2. Eckert, E. R. G.; Schneider, P. J.: Mass-Transfer Cooling in High-Speed Laminar Couette Flow, University of Minnesota. Tech. Rep. No. 12, April 1957.

3. Simon, H. A.; Liu, C. S.; Hartnett, J. P.; Chang, C. L.: Binary Couette Flow With Hydrogen Injection Into Carbon Dioxide and Nitrogen Streams, NASA Grant NSG 356, June 1964.

4. Scala, S. M.: The Equations of Motion in a Multicomponent Chemically Reacting Gas, General Electric Company, Document No. 58SD600, December 1957.

5. Schlichting, H.: Boundary Layer Theory, Fourth Edition, McGraw-Hill, New York.

6. Lees, L.: Convective Heat Transfer With Mass Addition and Chemical Reactions, Presented at the Fluid Combustion and Propulsion Colloquim, AGARD, NATO, Palmero, Italy, March 17-21, 1958.

7. Anon: JANAF Thermochemical Tables, Contract No. AF33(616)-6149, Thermal Laboratory, The Dow Chemical Company, June 30, 1962.

8. Zeleznik, F. J.; Gordon, S.: A General IBM 704 or 7090 Computer Program for Computation of Chemical Equilibrium Compositions, Rocket Performance, and Chapman-Jouguet Detonations, NASA TN D-1454, October 1962.

9. Hirschfelder, J. O.; Curtiss, C. F.; Bird, R. B.: Molecular Theory of Gases and Liquids, Second Edition, John Wiley and Sons, Inc., New York, 1964.

10. Brokaw, R. S.: Energy Transport in High Temperature and Reacting Gases, Air Force Office of Scientific Research - General Electric Company Conference of Physical Chemistry in Aerodynamics and Space Flight, Philadelphia, Pa., September 1-3, 1959.

11. Svehla, R. A.: Estimated Viscosities and Thermal Conductivities of Gases at High Temperatures, NASA TR R-132, 1962.

12. Knuth, E. L.: Multicomponent Diffusion and Fick's Law, Physics of Fluids, Vol. 2, 1959.

13. Hamming, R. W.: Numerical Methods for Scientists and Engineers, McGraw-Hill Book Co., New York, 1962.

14. Crandall, S. H.: Engineering Analysis, McGraw-Hill Book Co., New York, 1956.

15. Smith, A. M. O.; Clutter, D. W.: Machine Calculation of Compressible Laminar Boundary Layers, AIAA Journal, Vol. 3, No. 4, April 1965, pp. 639-647.

16. Henrici, P.: Elements of Numerical Analysis, John Wiley and Sons, Inc., New York, 1964.

17. Milne, W. E.: Numerical Solution of Differential Equations, John Wiley and Sons, Inc., New York, 1953.

VITA

The author was born in Norfolk, Virginia, on February 16, 1939. He attended school in Norfolk, Virginia, and was graduated from Granby High School in June 1958.

Upon graduation from high school he entered the Norfolk Division of Virginia Polytechnic Institute to pursue a bachelor of science degree in Mechanical Engineering. In the fall of 1961 the author transferred to Virginia Polytechnic Institute and remained there until June 1963 at which time he received a bachelor of science degree in Mechanical Engineering.

After graduation he was employed by the National Aeronautics and Space Administration, Langley Research Center, Hampton, Virginia, and is presently assigned to the Thermodynamics and Combustion Section of the Aerothermochemistry Branch in the Applied Materials and Physics Division.

The author is married to the former Stephanie Thompson and has one child. He and his family reside at 2307 N. Armistead Avenue, Hampton, Virginia.

APPENDIX A

THREE-POINT DERIVATIVE FORMULAS

Figure 32 shows the finite-difference stations in the Couette flow and for the present analysis these stations are evenly spaced. The distance between stations is $\Delta\eta$. The finite-difference form of the first derivative is obtained by a Taylor series expansion about station N evaluated at stations N+1 and N-1, with

$$F_{N+1} = F_N + \Delta\eta\left(\frac{dF}{d\eta}\right)_N + \frac{(\Delta\eta)^2}{2}\left(\frac{d^2F}{d\eta^2}\right)_N + \frac{(\Delta\eta)^3}{6}\left(\frac{d^3F}{d\eta^3}\right)_N$$

and

$$F_{N-1} = F_N - \Delta\eta\left(\frac{dF}{d\eta}\right)_N + \frac{(\Delta\eta)^2}{2}\left(\frac{d^2F}{d\eta^2}\right)_N - \frac{(\Delta\eta)^3}{6}\left(\frac{d^3F}{d\eta^3}\right)_N$$

Solving for the first derivative $\left(\frac{dF}{d\eta}\right)_N$

$$\left(\frac{dF}{d\eta}\right)_N = \frac{F_{N+1} - F_{N-1}}{2\Delta\eta} - \frac{(\Delta\eta)^3}{6}\left(\frac{d^3F}{d\eta^3}\right)_N$$

The first derivative is thus correct to terms of order $(\Delta\eta)^3$.

The first derivative at the lower boundary (N = 1) is also determined by the Taylor series expansion about station N but is evaluated at stations N+1 and N+2, with

$$F_{N+1} = F_N + \Delta\eta\left(\frac{dF}{d\eta}\right)_N + \frac{(\Delta\eta)^2}{2}\left(\frac{d^2F}{d\eta^2}\right)_N + \frac{(\Delta\eta)^3}{6}\left(\frac{d^3F}{d\eta^3}\right)_N$$

and

$$F_{N+2} = F_N + 2\Delta\eta\left(\frac{dF}{d\eta}\right)_N + \frac{4}{2}(\Delta\eta)^2\left(\frac{d^2F}{d\eta^2}\right)_N + \frac{8}{6}(\Delta\eta)^3\left(\frac{d^3F}{d\eta^3}\right)_N$$

Solving for the first derivative $\left(\frac{dF}{d\eta}\right)_N$

$$\left(\frac{dF}{d\eta}\right)_{N=1} = \frac{4F_{N+1} - 3F_N - F_{N+2}}{2\Delta\eta} + \frac{2}{3}(\Delta\eta)^3\left(\frac{d^3F}{d\eta^3}\right)_{N=1}$$

The first derivative is again correct to terms of order $(\Delta\eta)^3$.

In a similar manner solving for the first derivative at the upper boundary (N = NT):

$$\left(\frac{dF}{d\eta}\right)_{N=NT} = \frac{3F_N + F_{N-2} - 4F_{N-1}}{2\Delta\eta} + \frac{2}{3}(\Delta\eta)^3\left(\frac{d^3F}{d\eta^3}\right)_{N=NT}$$

Likewise the first derivative at the upper boundary is correct to terms of order $(\Delta\eta)^3$.

The above formulas are used in the solid wall calculations wherever a first derivative is needed.

APPENDIX B

FOUR-POINT DERIVATIVE FORMULAS

As in the case of the three-point derivative formulas the finite-difference points are evenly spaced as shown in figure 32. The finite-difference form of the first derivative at station N is obtained by a Taylor series expansion about station N and is evaluated at stations N-1, N+1, N+2. Thus:

$$F_{N-1} = F_N - \Delta\eta\left(\frac{dF}{d\eta}\right)_N + \frac{(\Delta\eta)^2}{2}\left(\frac{d^2F}{d\eta^2}\right)_N - \frac{(\Delta\eta)^3}{}\left(\frac{d^3F}{d\eta^3}\right)_N + - - - -$$

$$F_{N+1} = F_N + \Delta\eta\left(\frac{dF}{d\eta}\right)_N + \frac{(\Delta\eta)^2}{2}\left(\frac{d^2F}{d\eta^2}\right)_N + \frac{(\Delta\eta)^3}{6}\left(\frac{d^3F}{d\eta^3}\right)_N + - - - -$$

$$F_{N+2} = F_N + 2\Delta\eta\left(\frac{dF}{d\eta}\right)_N + \frac{4}{2}(\Delta\eta)^2\left(\frac{d^2F}{d\eta^2}\right)_N + \frac{8}{6}(\Delta\eta)^3\left(\frac{d^3F}{d\eta^3}\right)_N + - - - -$$

Solving for the first derivative $\left(\frac{dF}{d\eta}\right)_N$

$$\left(\frac{dF}{d\eta}\right)_N = \frac{1}{6\Delta\eta}\left\{6F_{N+1} - 3F_N - 2F_{N-1} - F_{N+2}\right\} + \frac{(\Delta\eta)^3}{12}\left(\frac{d^4F}{d\eta^4}\right)_N$$

The first derivative is correct to terms of order $(\Delta\eta)^3$. The above equation applies in the interval $2 \leq N \leq NT - 2$.

At station $N = NT - 1$ the first derivative is again obtained from the Taylor series expansion but is evaluated at stations N-2, N-1, and N+1, giving:

$$F_{N-2} = F_N - 2\Delta\eta\left(\frac{dF}{d\eta}\right)_N + \frac{4}{2}(\Delta\eta)^2\left(\frac{d^2F}{d\eta^2}\right)_N - \frac{8}{6}(\Delta\eta)^3\left(\frac{d^3F}{d\eta^3}\right)_N + - - - -$$

$$F_{N-1} = F_N - \Delta\eta\left(\frac{dF}{d\eta}\right)_N + \frac{(\Delta\eta)^2}{2}\left(\frac{d^2F}{d\eta^2}\right)_N - \frac{(\Delta\eta)^3}{6}\left(\frac{d^3F}{d\eta^3}\right)_N + - - - -$$

$$F_{N+1} = F_N + \Delta\eta\left(\frac{dF}{d\eta}\right)_N + \frac{(\Delta\eta)^2}{2}\left(\frac{d^2F}{d\eta^2}\right)_N + \frac{(\Delta\eta)^3}{6}\left(\frac{d^3F}{d\eta^3}\right)_N + - - - -$$

Solving for the first derivative $\left(\frac{dF}{d\eta}\right)_N$

$$\left(\frac{dF}{d\eta}\right)_N = \frac{1}{6\Delta\eta}\left\{2F_{N+1} + 3F_N - 6F_{N-1} + F_{N-2}\right\} + \frac{(\Delta\eta)^3}{12}\left(\frac{d^4F}{d\eta^4}\right)_N$$

Again the first derivative is correct to terms of order $(\Delta\eta)^3$ and the above equation applies only at $N = NT - 1$.

At the lower boundary ($N = 1$) the first derivative is again obtained from a Taylor series expansion about station 1 but evaluated at stations N+1, N+2, and N+3. Thus:

$$F_{N+1} = F_N + \Delta\eta\left(\frac{dF}{d\eta}\right)_N + \frac{(\Delta\eta)^2}{d\eta^2}\left(\frac{d^2F}{d\eta^2}\right)_N + \frac{(\Delta\eta)^3}{6}\left(\frac{d^3F}{d\eta^3}\right)_N + - - - -$$

$$F_{N+2} = F_N + 2\Delta\eta\left(\frac{dF}{d\eta}\right)_N + \frac{4}{2}(\Delta\eta)^2\left(\frac{d^2F}{d\eta^2}\right)_N + \frac{8}{6}(\Delta\eta)^3\left(\frac{d^3F}{d\eta^3}\right)_N + - - - -$$

$$F_{N+3} = F_N + 3\Delta\eta\left(\frac{dF}{d\eta}\right)_N + \frac{9}{2}(\Delta\eta)^2\left(\frac{d^2F}{d\eta^2}\right)_N + \frac{27}{6}(\Delta\eta)^3\left(\frac{d^3F}{d\eta^3}\right)_N + - - - -$$

Solving for the first derivative $\left(\frac{dF}{d\eta}\right)_N$

$$\left(\frac{dF}{d\eta}\right)_N = \frac{1}{6\Delta\eta}\left\{-11F_N + 18F_{N+1} - 9F_{N+2} + 2F_{N+3}\right\} + \frac{(\Delta\eta)^3}{4}\left(\frac{d^4F}{d\eta^4}\right)_N$$

Again the first derivative is correct to terms of order $(\Delta\eta)^3$. In a similar manner solving for the first derivative at the upper boundary (N = NT):

$$\left(\frac{dF}{d\eta}\right)_N = \frac{1}{6\Delta\eta}\left\{11T_N - 18T_{N-1} + 9T_{N-2} - 2T_{N-3}\right\} + \frac{(\Delta\eta)^3}{4}\left(\frac{d^4F}{d\eta^4}\right)_N$$

Likewise the first derivative at the upper boundary is correct to terms of order $(\Delta\eta)^3$.

The above equations are used in the calculation of a first derivative wherever one is needed in the solution of the equations governing Couette flow with injection.

APPENDIX C

SIX-POINT INTEGRATION FORMULAS

The six-point integration formulas given by Milne in reference 17 and rearranged for the present analysis are:

N = 2

$$F_2 = F_1 + \frac{\Delta\eta}{1440.}\left\{493.\ f_1 + 1337.\ f_2 - 618.\ f_3 + 302.\ f_4 - 82.\ f_5 + 9.\ f_6\right\}$$

where the error term is:

$$\frac{-862.\ (\Delta\eta)^7}{60{,}480.}\left(\frac{d^7F}{d\eta^7}\right)_N$$

N = 3

$$F_3 = F_2 + \frac{\Delta\eta}{129600.}\left\{-4050.\ f_1 + 65430.\ f_2 + 75780.\ f_3 - 7020.\ f_4 - 1170.\ f_5 + 630.\ f_6\right\}$$

with the error being:

$$\frac{-77481.}{6048.}\ (\Delta\eta)^7\left(\frac{d^7F}{d\eta^7}\right)_N$$

From N = 4 to NT - 2

$$F_N = F_{N-1} + \frac{\Delta\eta}{14400.}\left\{110.\ f_{N-3} - 930.\ f_{N-2} + 8020.\ f_{N-1} + 8020\ f_N - 930.\ f_{N+1} + 110.\ f_{N+2}\right\}$$

the error term is:

$$+ \frac{16975.}{42336.}(\Delta\eta)^7\left(\frac{d^7F}{d\eta^7}\right)_N$$

N + NT - 1

$$F_N = F_{N-1} + \frac{\Delta\eta}{14400.}\left\{-110.\ f_{N-4} + 770.\ f_{N-3} - 2580.\ f_{N-2} + 10220.\ f_{N-1} + 6370.\ f_N - 270.\ f_{N+1}\right\}$$

the error term is:

$$- \frac{8015.}{42336.}(\Delta\eta)^7\left(\frac{d^7F}{d\eta^7}\right)_N$$

N = NT

$$F_N = F_{N-1} + \frac{\Delta\eta}{25920.}\left\{486.\ f_{N-5} - 3114.\ f_{N-4} + 8676.\ f_{N-3} - 14364.\ f_{N-2} + 25686.\ f_{N-1} + 8550.\ f_N\right\}$$

the error term is:

$$+\frac{45027.}{20160.}(\Delta\eta)^7\left(\frac{d^7F}{d\eta^7}\right)_N$$

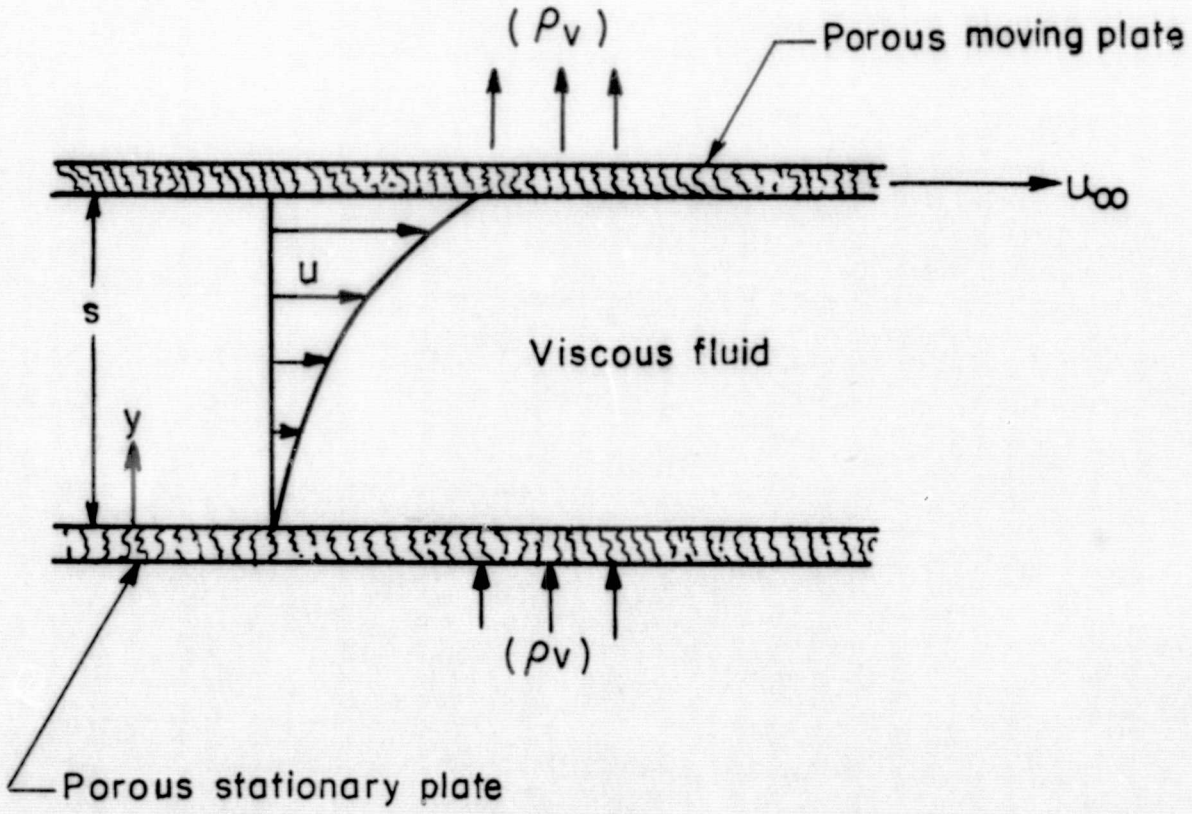

Figure 1.- Schematic of Couette flow.

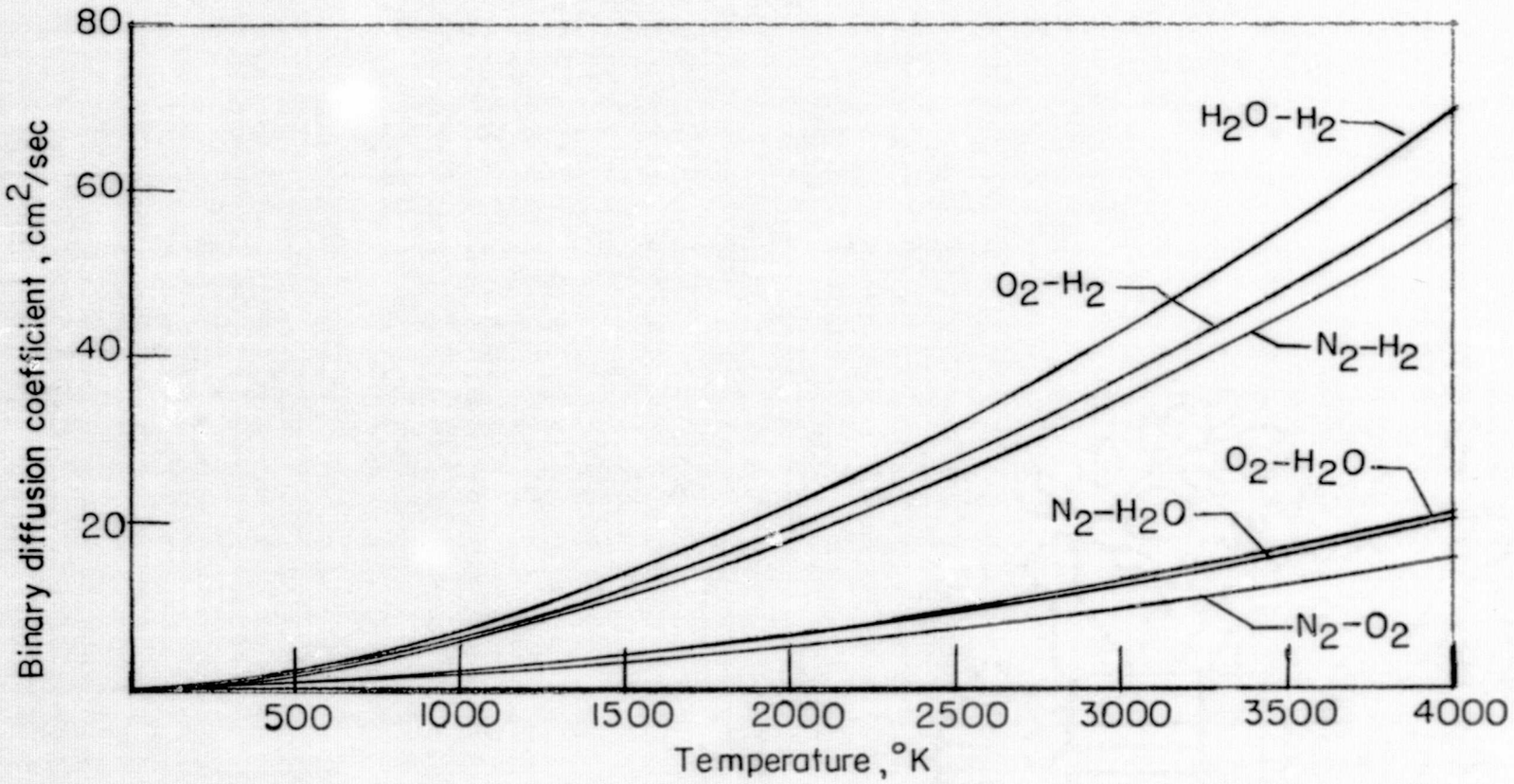

Figure 2.- Binary diffusion coefficients.

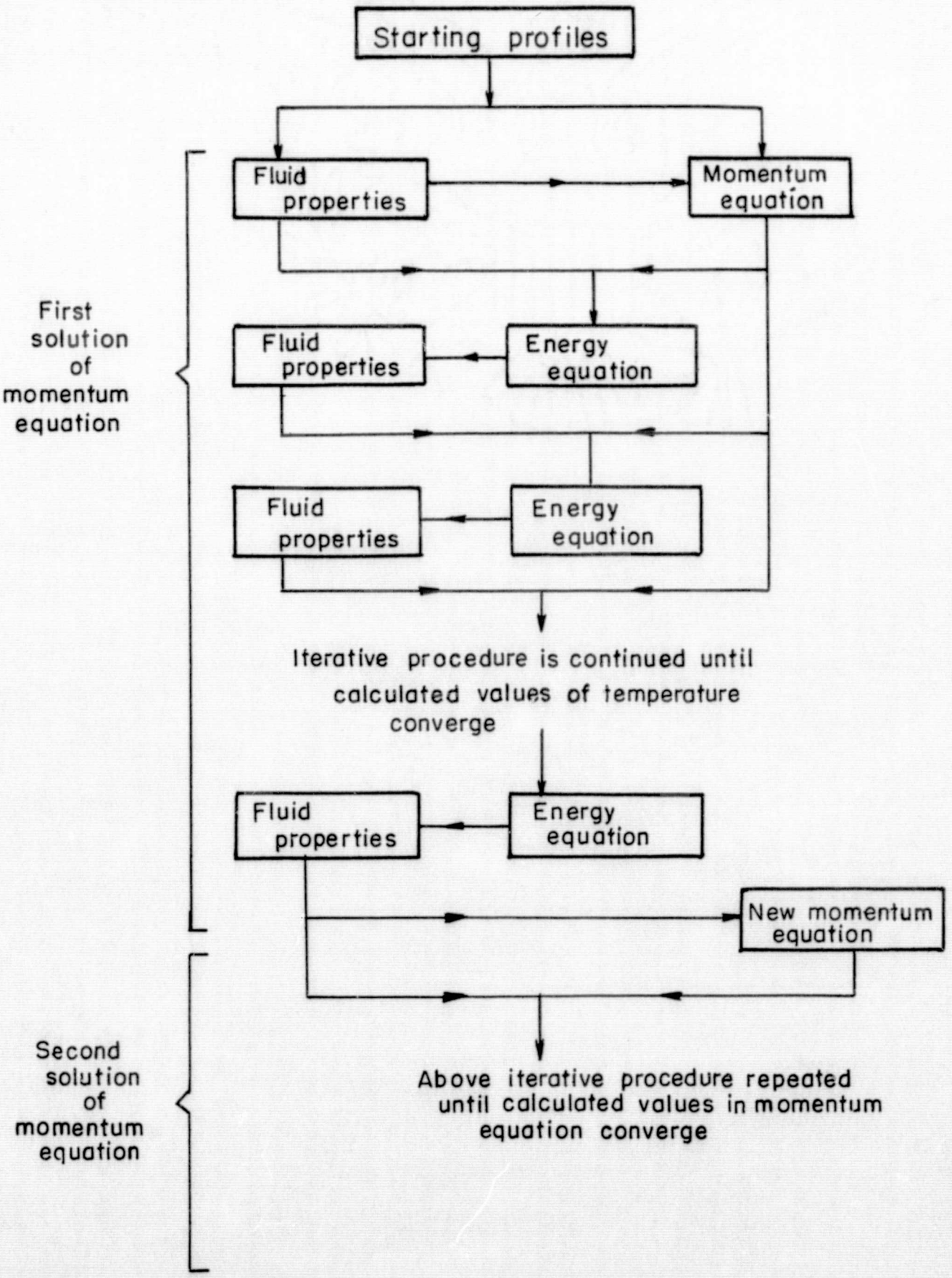

Figure 3.- Main iteration process.

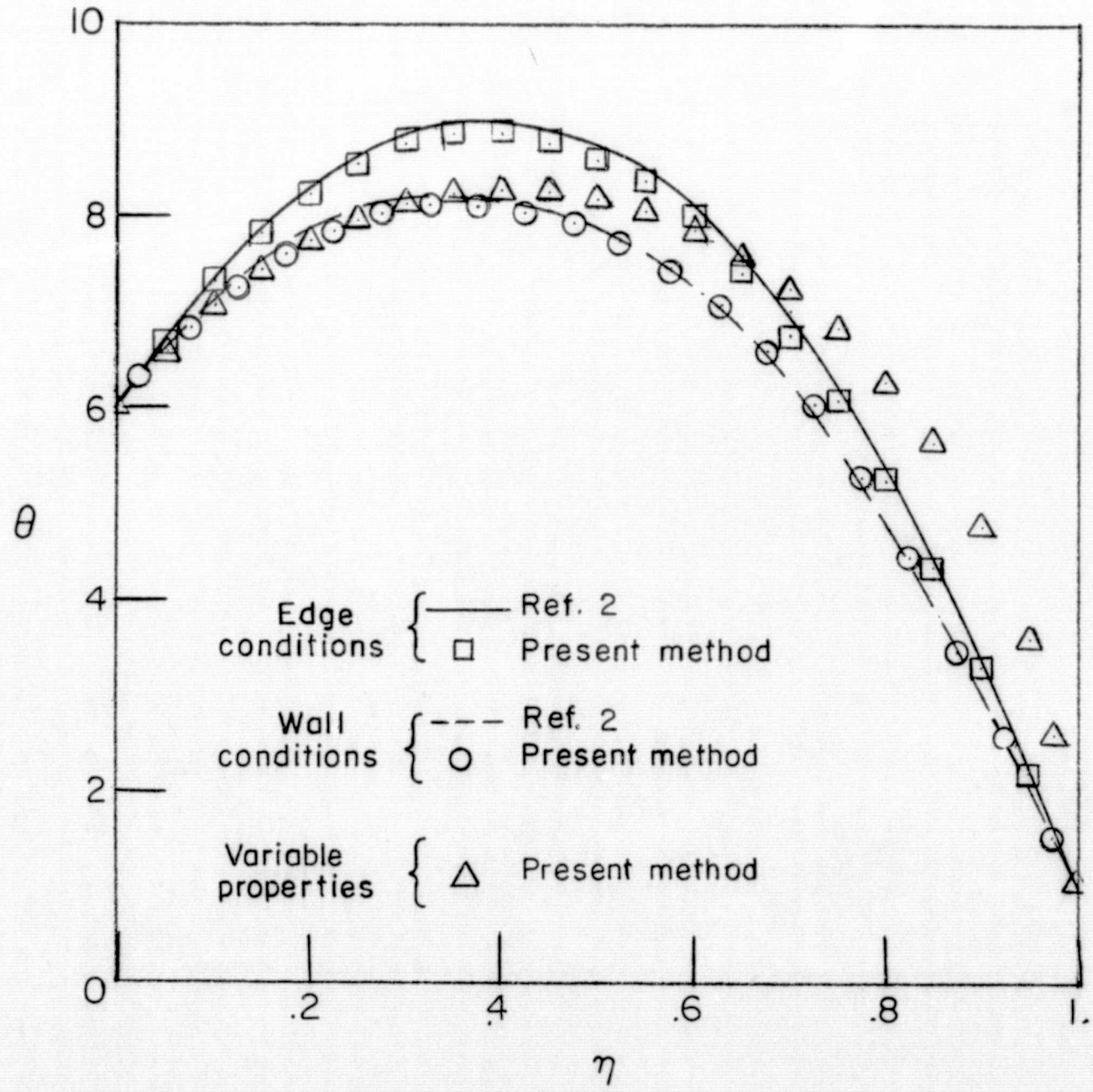

Figure 4.- Comparison for constant property Couette flow with no injection.

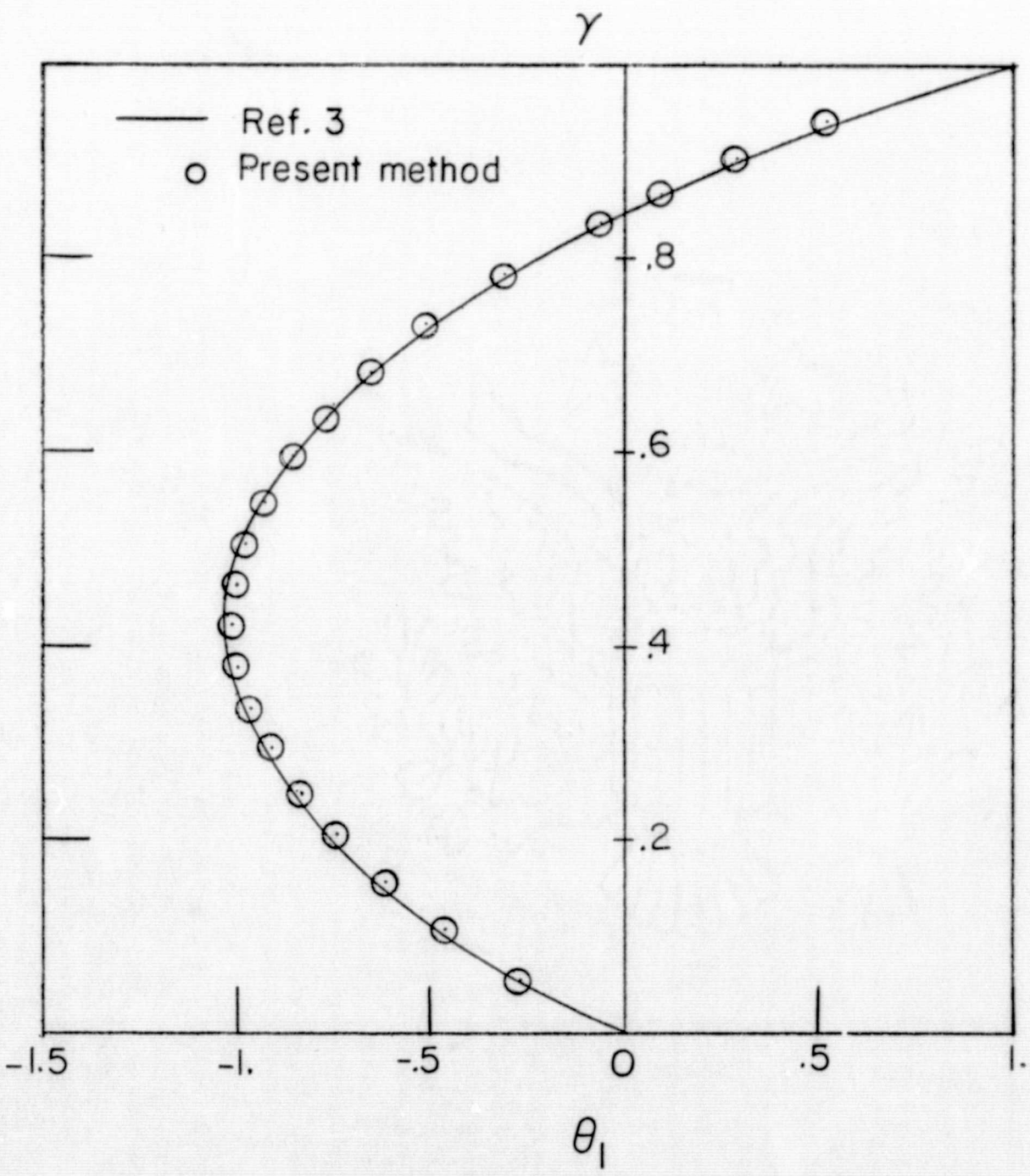

Figure 5.- Comparison for variable property Couette flow with no injection.

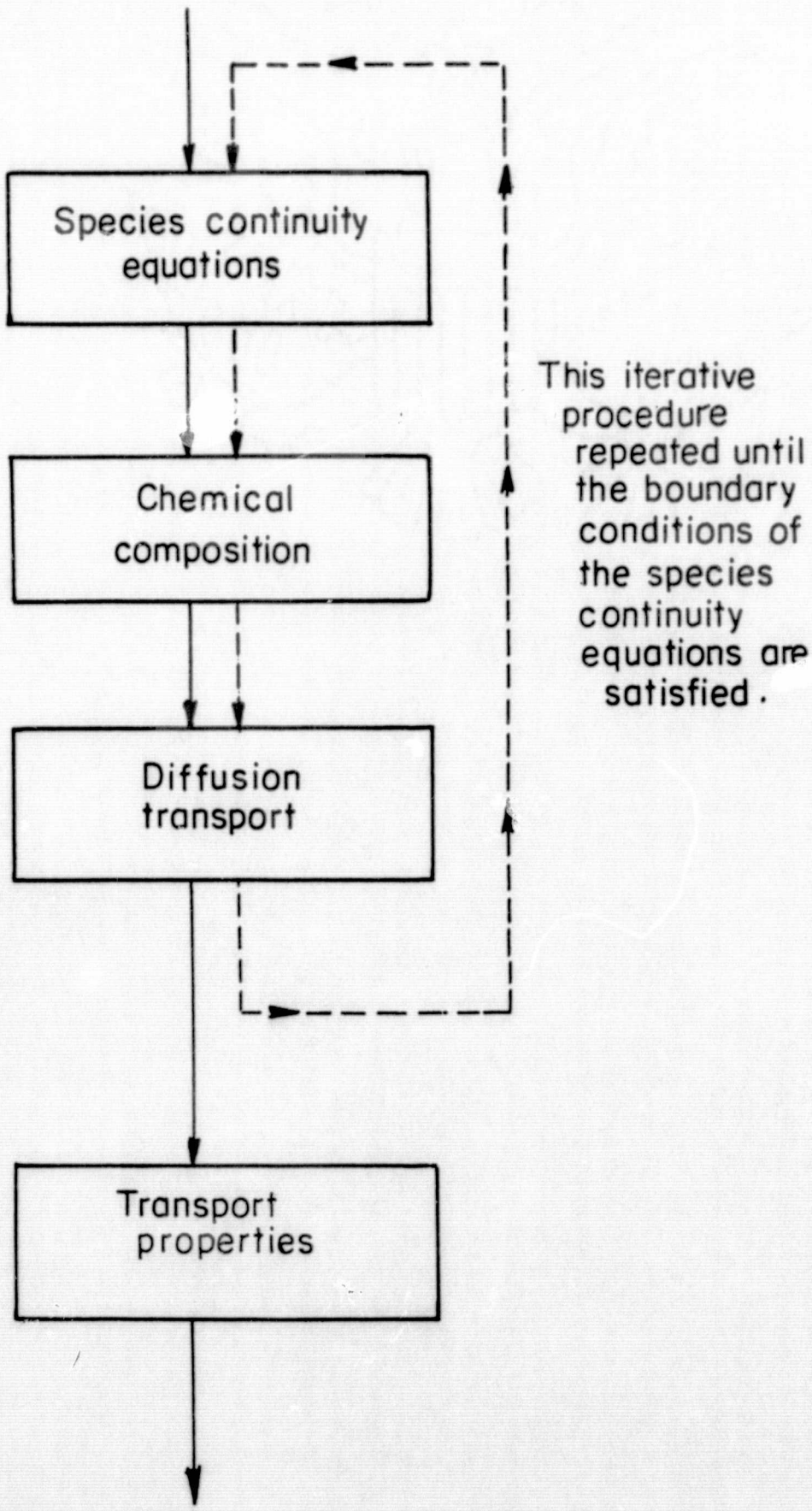

Figure 6.- Fluid properties iteration process.

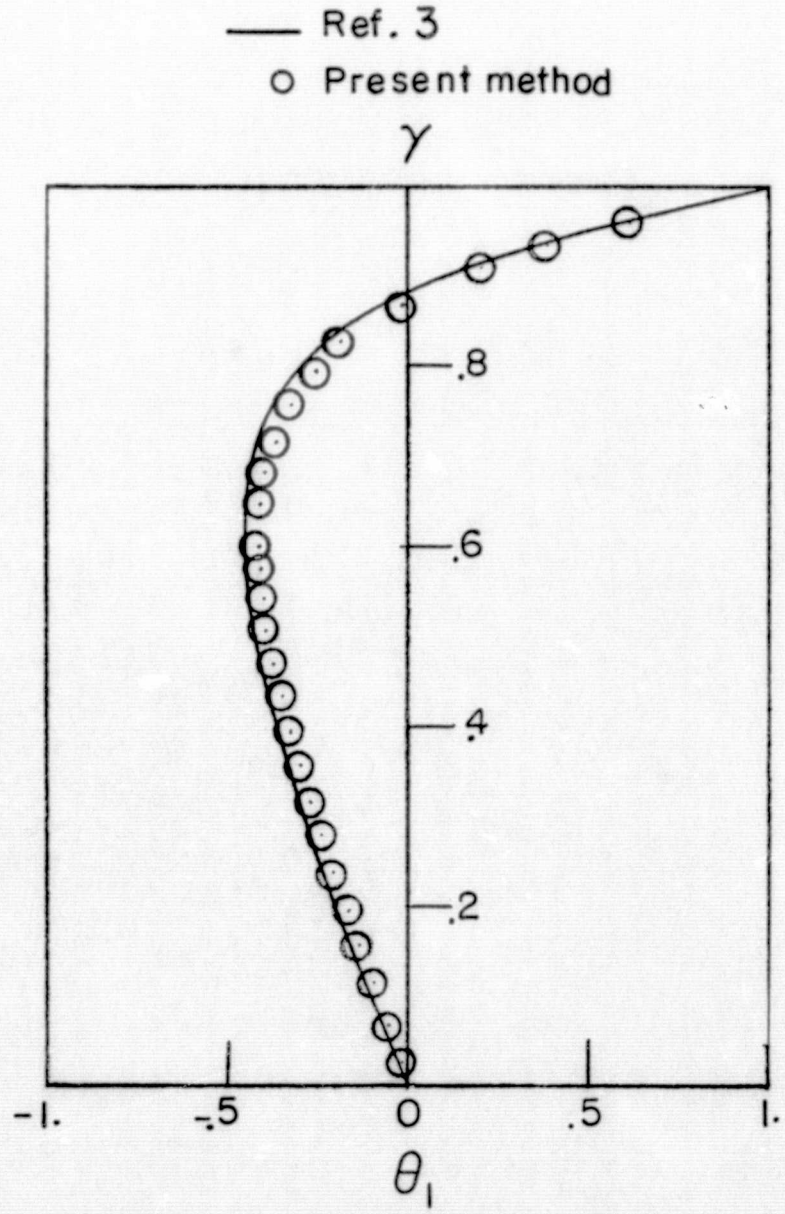

Figure 7.- Temperature profile comparison for nitrogen Couette flow with hydrogen injection.

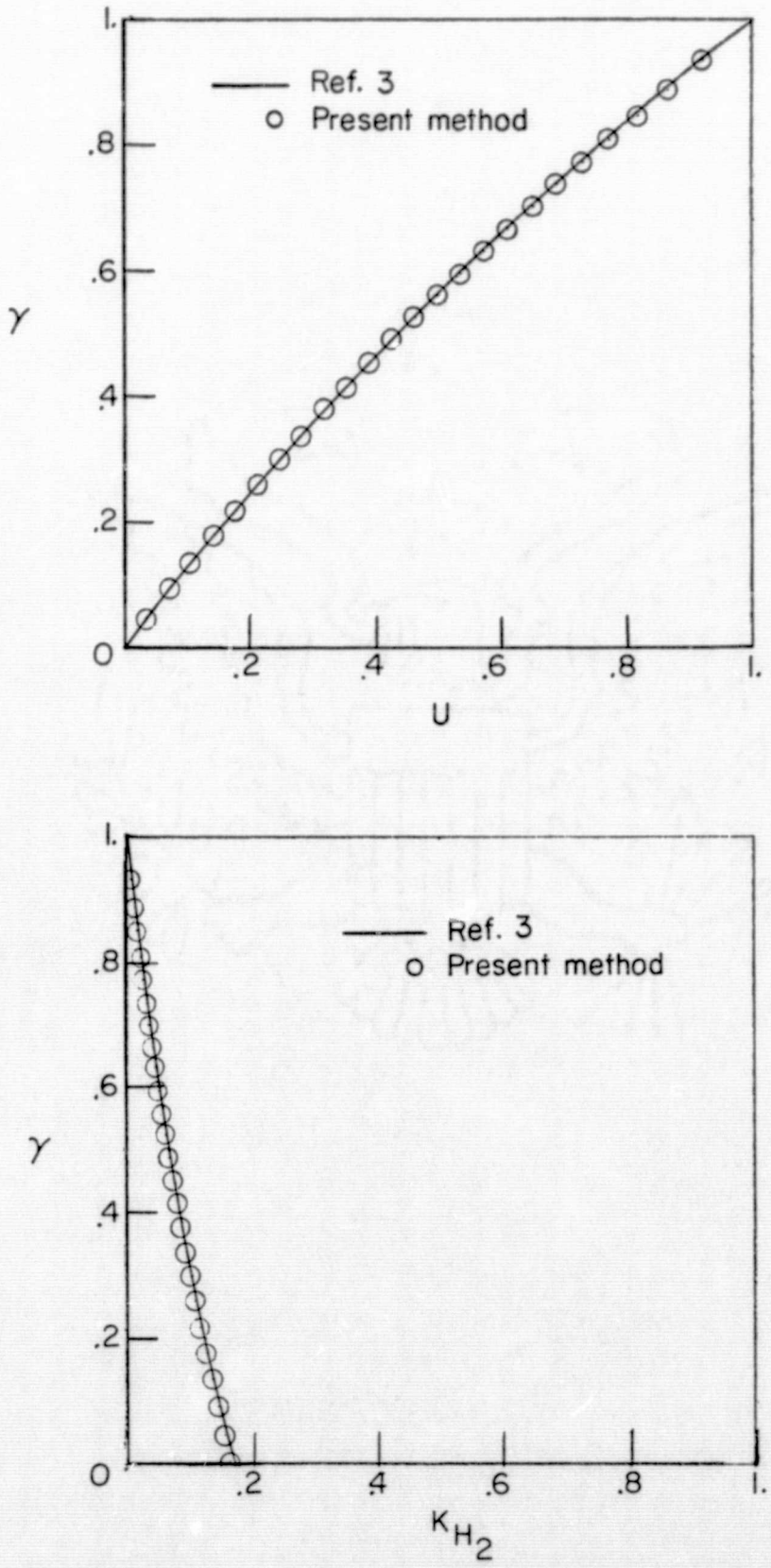

Figure 8.- Velocity and concentration profiles for nitrogen Couette flow with hydrogen injection.

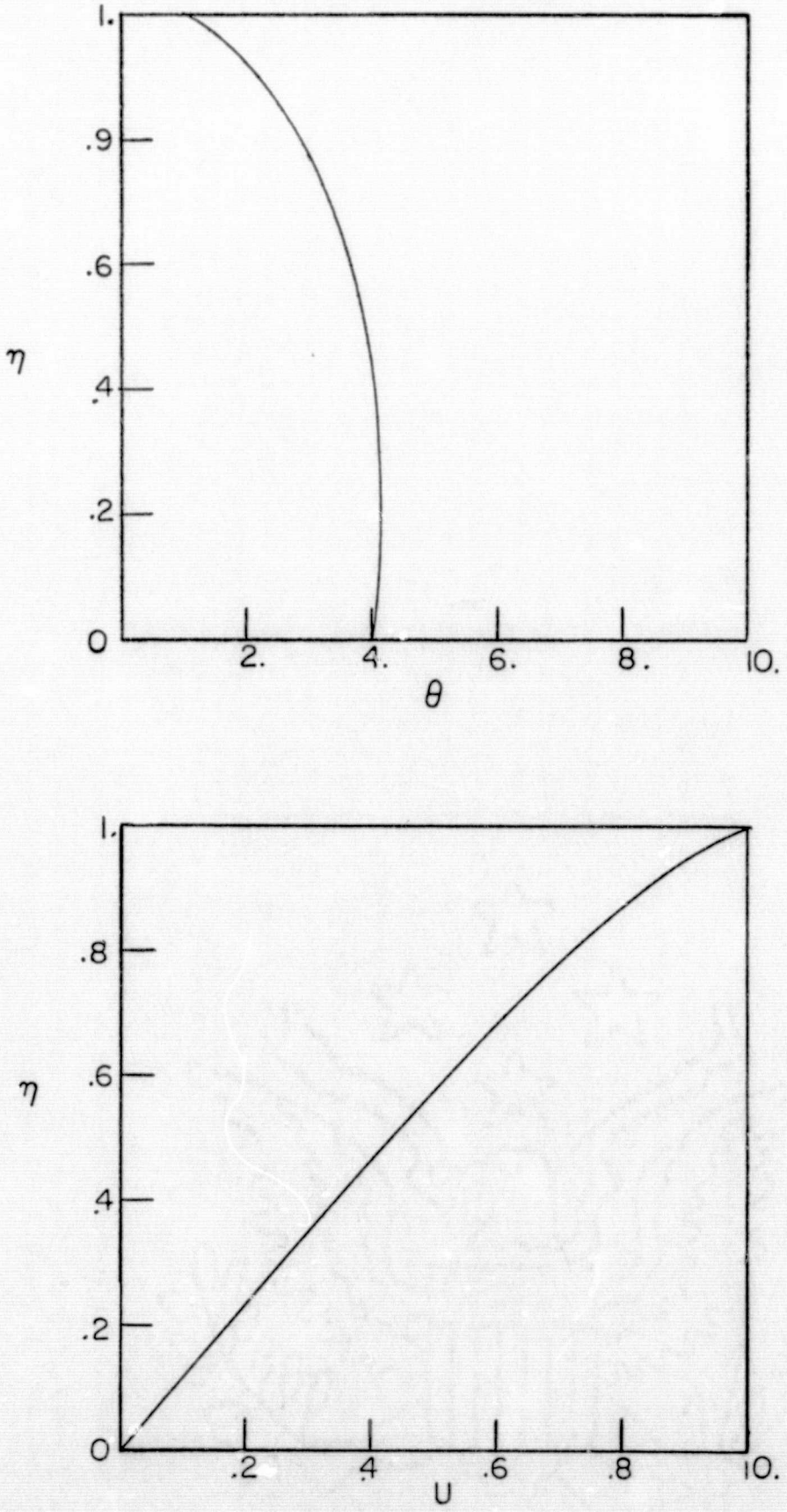

Figure 9.- Temperature and velocity profiles for air Couette flow with no injection.

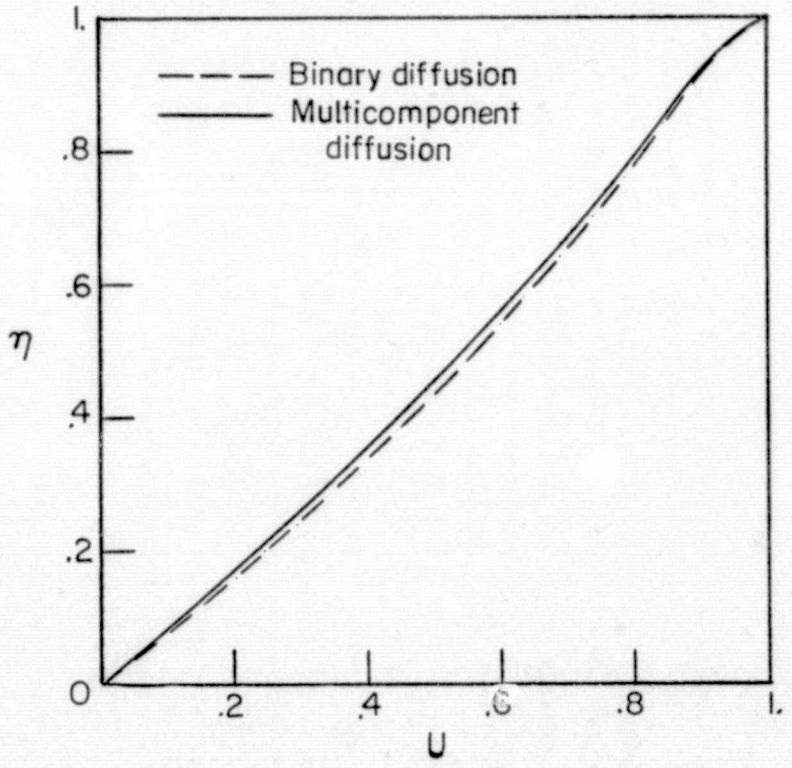

(a) $\delta_o = 1.3$

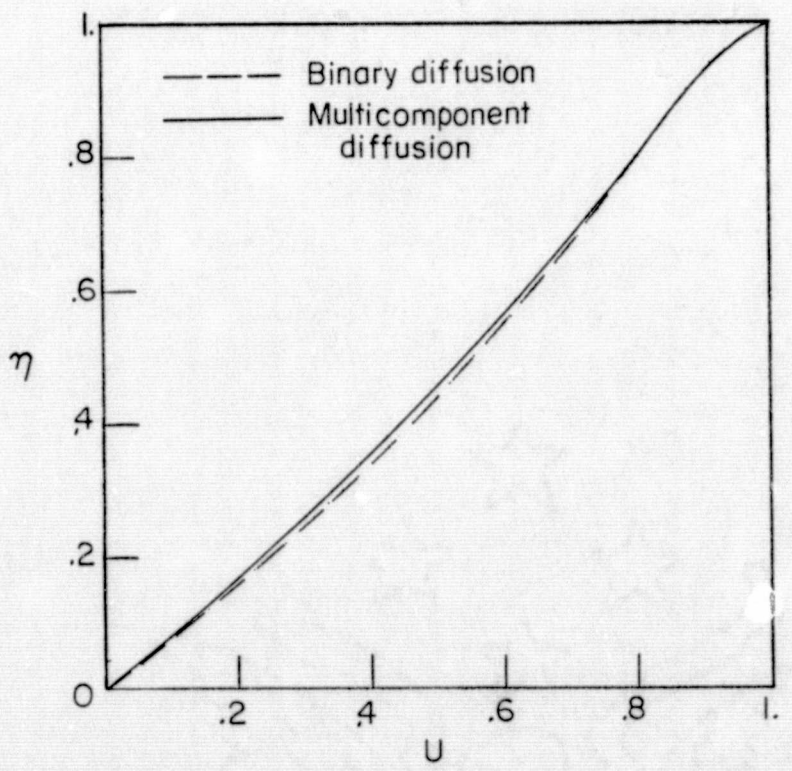

(b) $\delta_o = 1.0$

Figure 10.- Velocity profiles for $\delta_o = 1.3$ and 1.0.

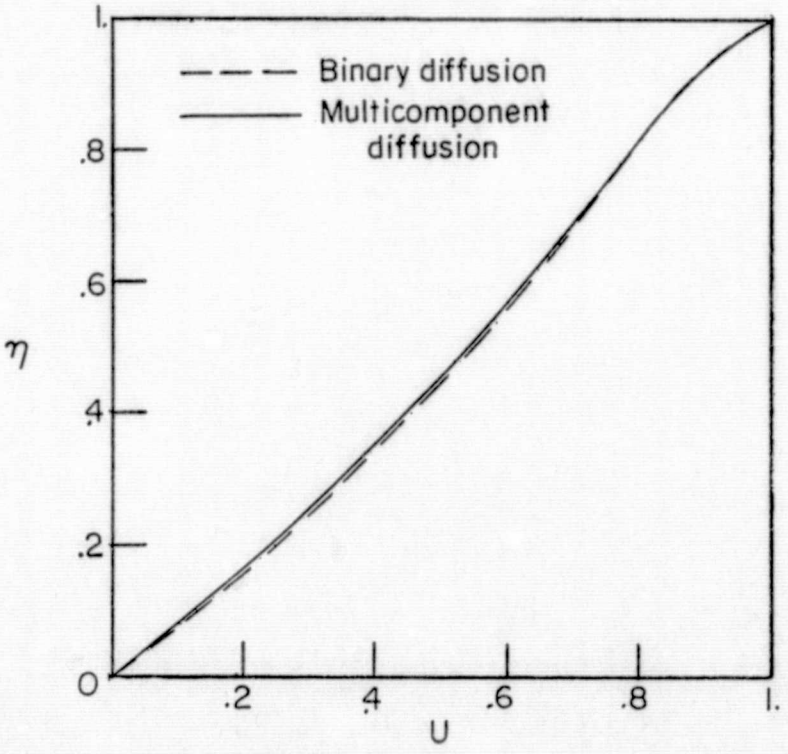

(a) $\delta_o = 0.75$

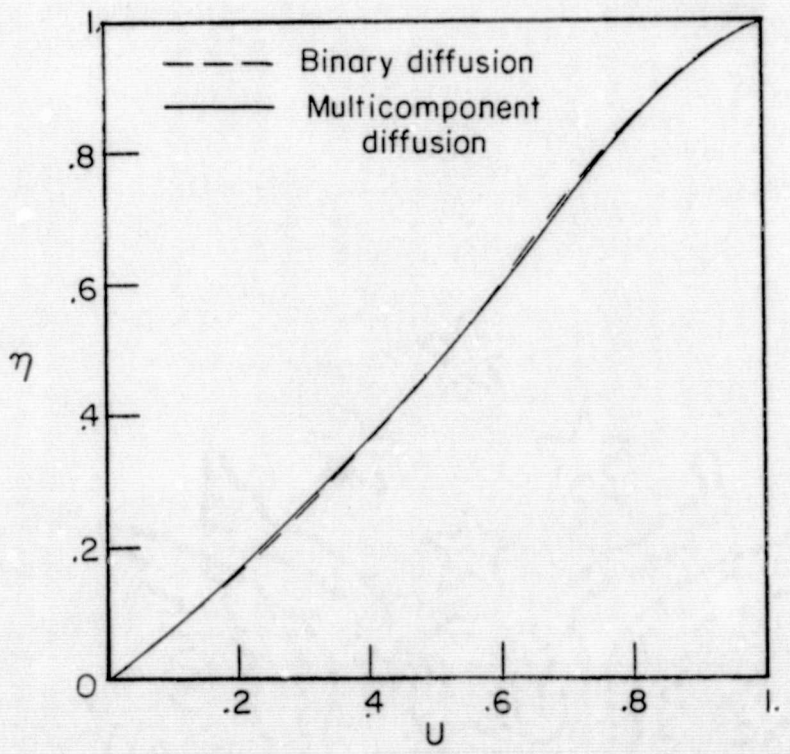

(b) $\delta_o = 0.5$

Figure 11.- Velocity profiles for $\delta_o = 0.75$ and 0.5.

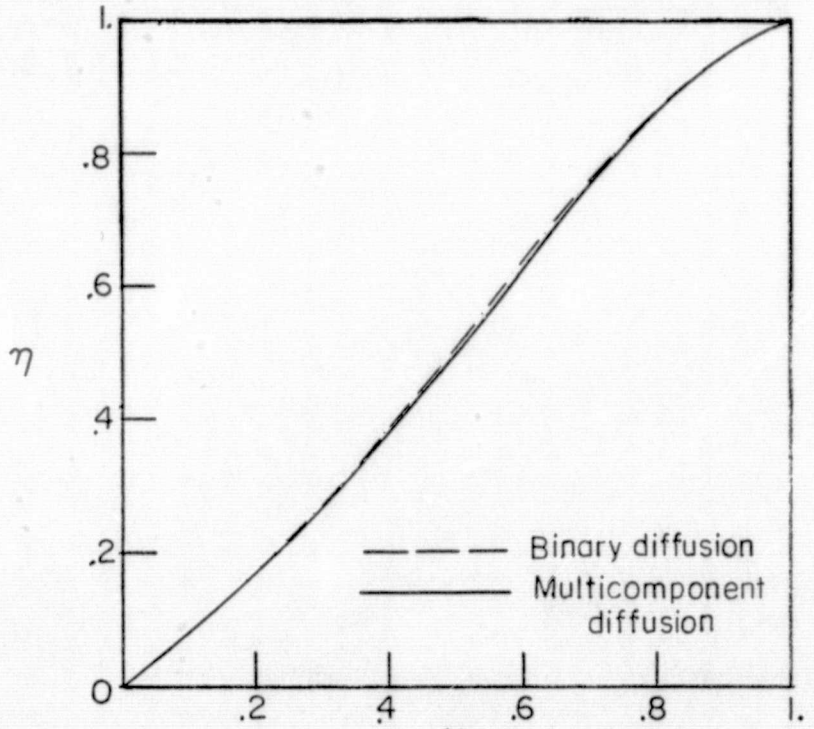

(a) $\delta_o = 0.35$

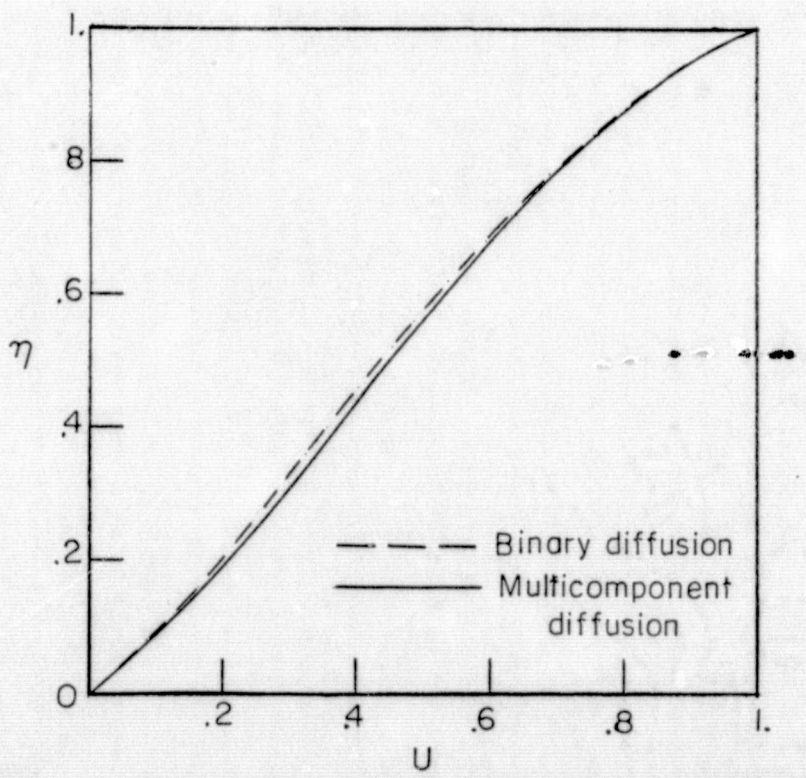

(b) $\delta_o = 0.2$

Figure 12.- Velocity profiles for $\delta_o = 0.35$ and 0.2.

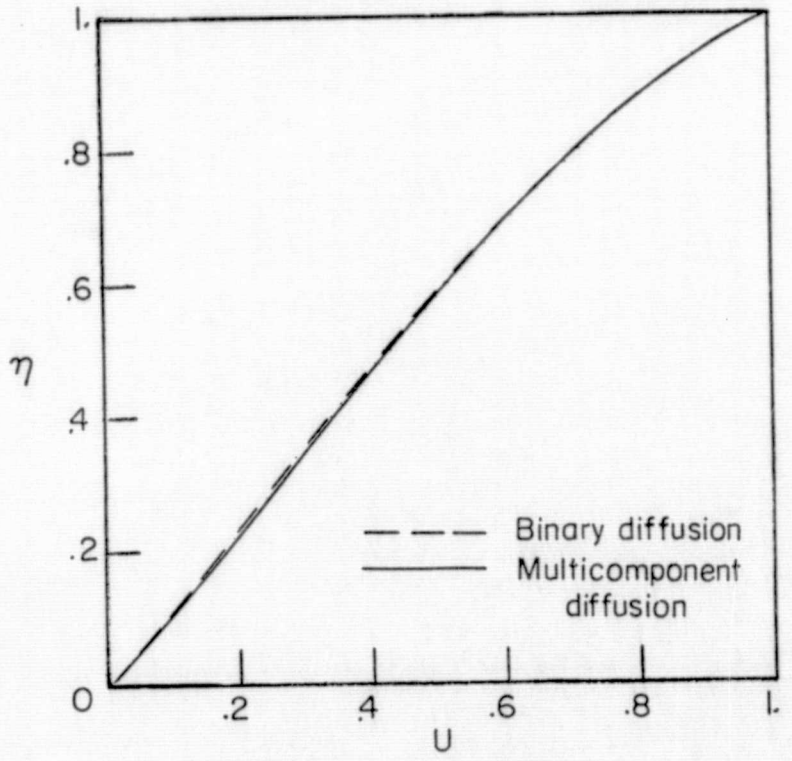

(a) $\delta_o = 0.13$

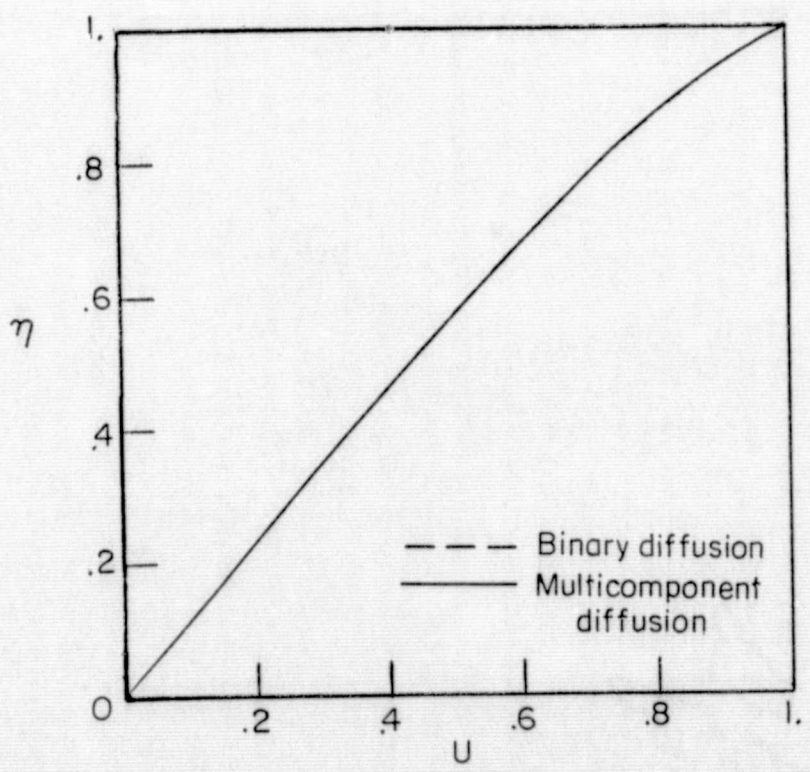

(b) $\delta_o = 0.1$

Figure 13.- Velocity profiles for $\delta_o = 0.13$ and 0.1.

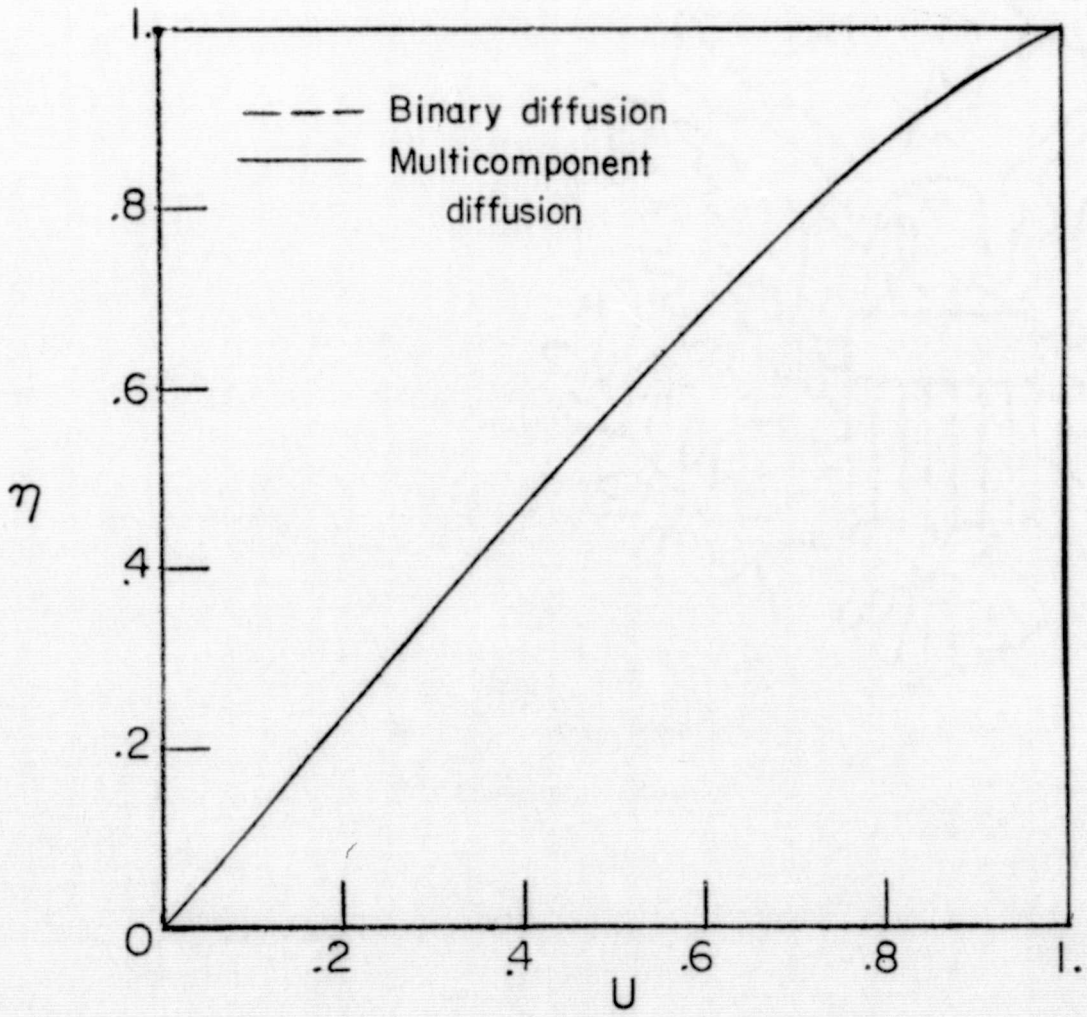

Figure 14.- Velocity profiles for $\delta_o = 0.05$.

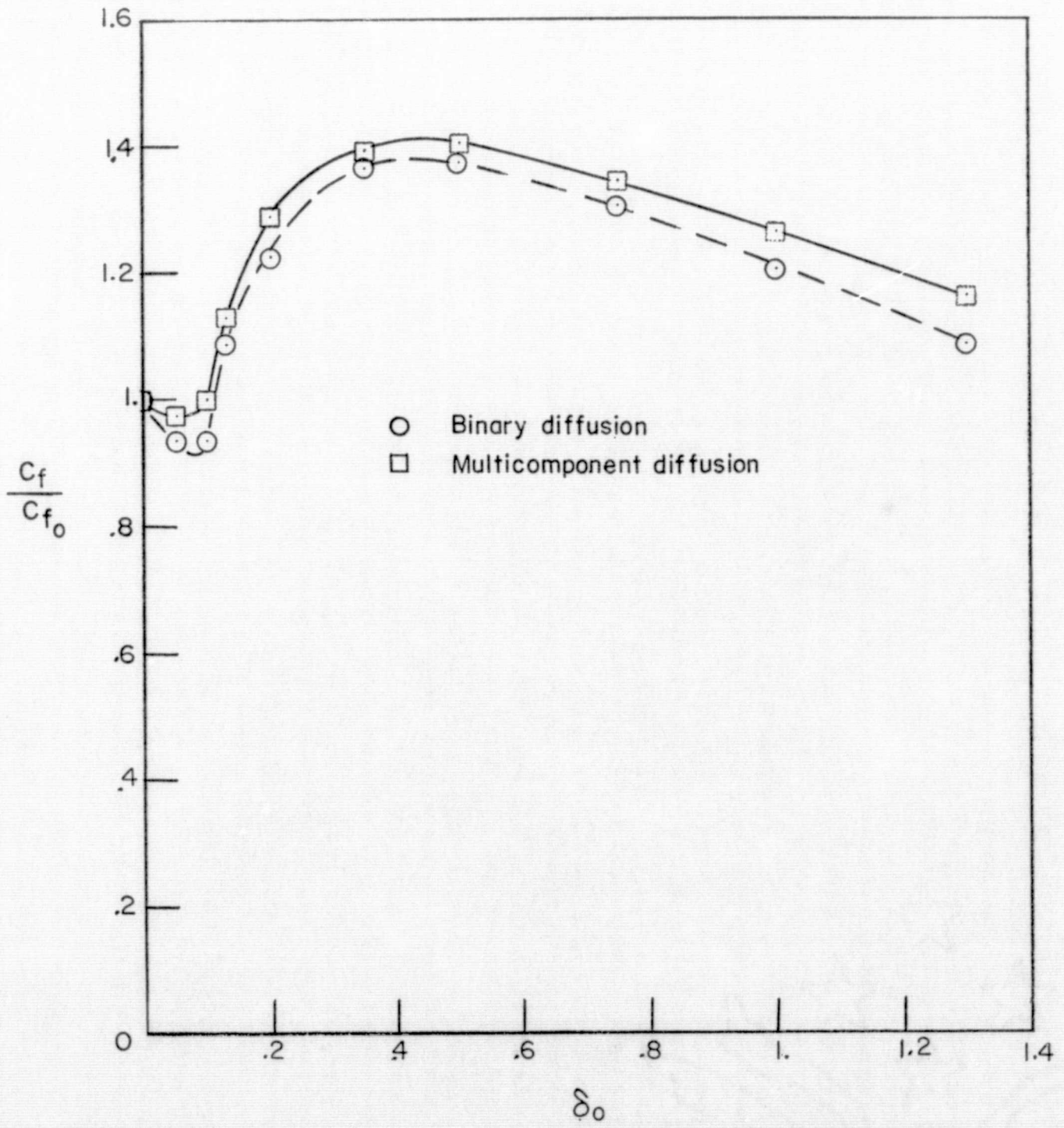

Figure 15.- Shear stress results.

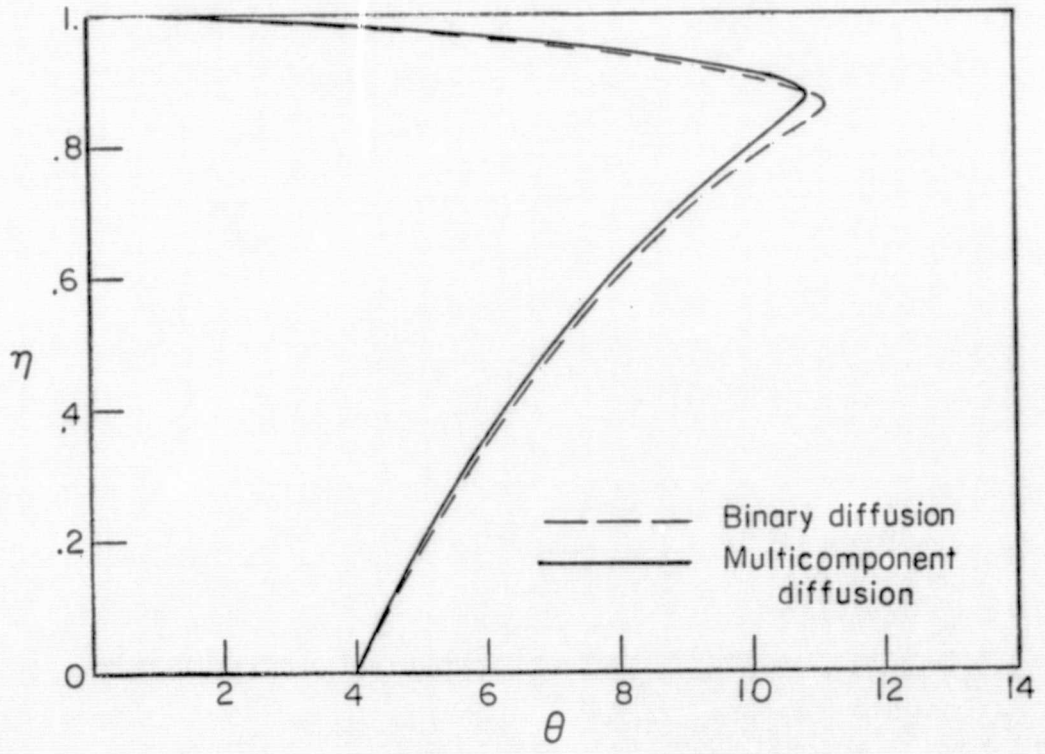

(a) $\delta_o = 1.3$

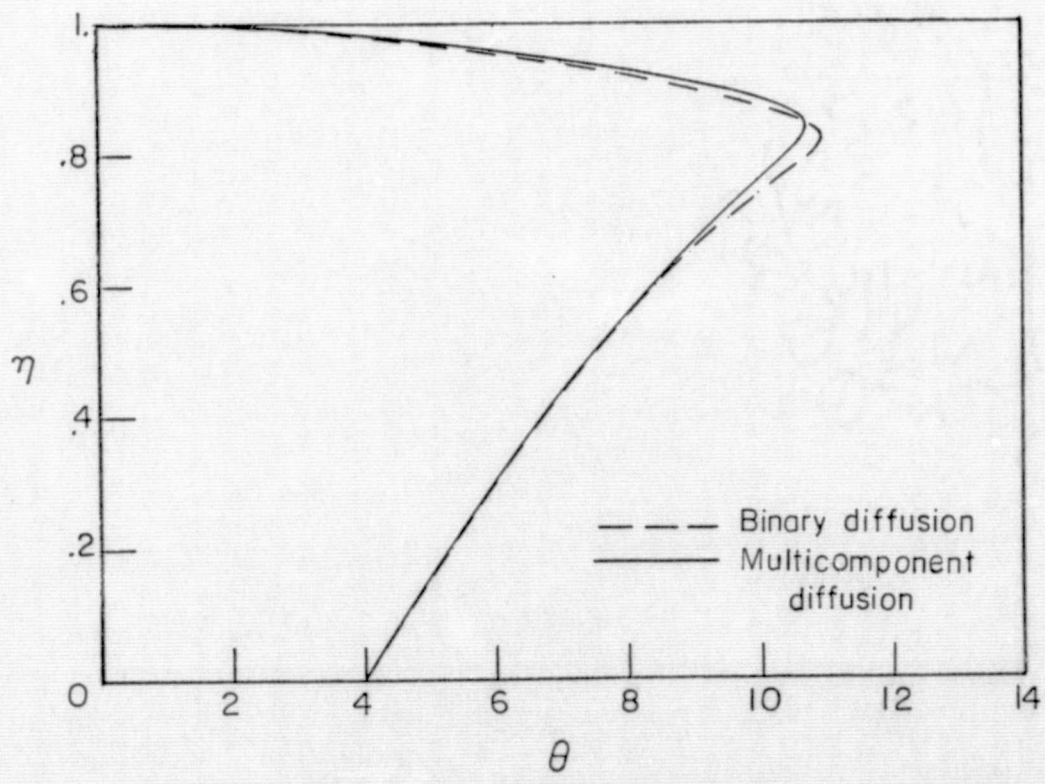

(b) $\delta_o = 1.0$

Figure 16.- Temperature profiles for $\delta_o = 1.3$ and 1.0.

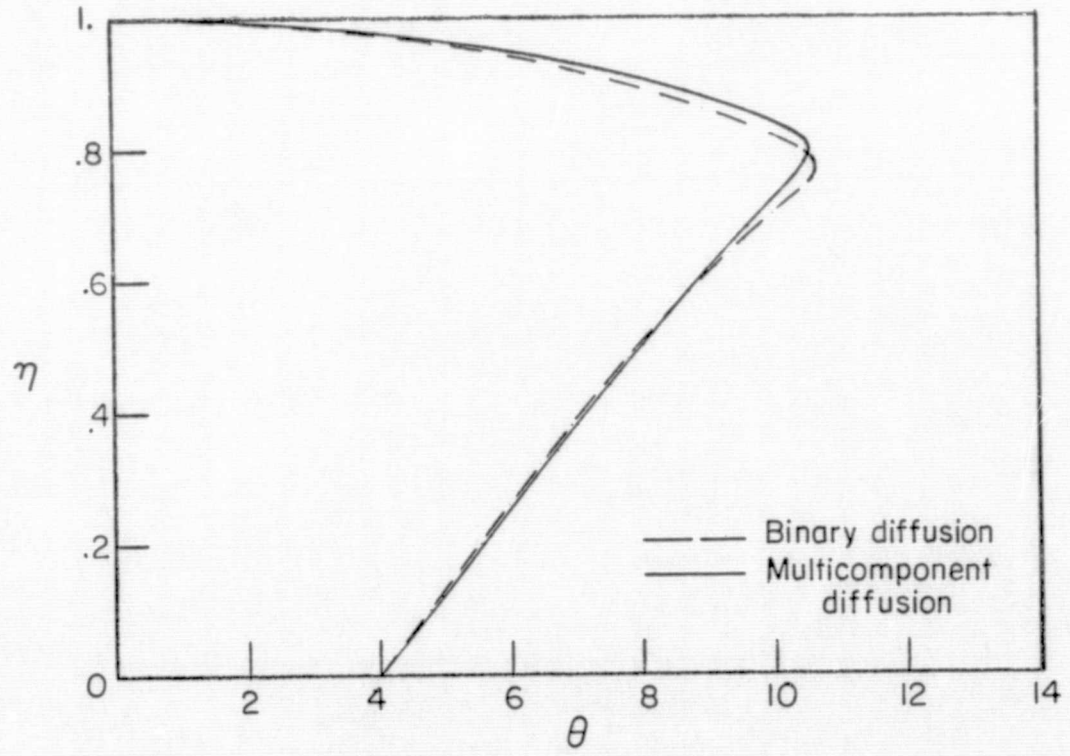

(a) $\delta_o = 0.75$

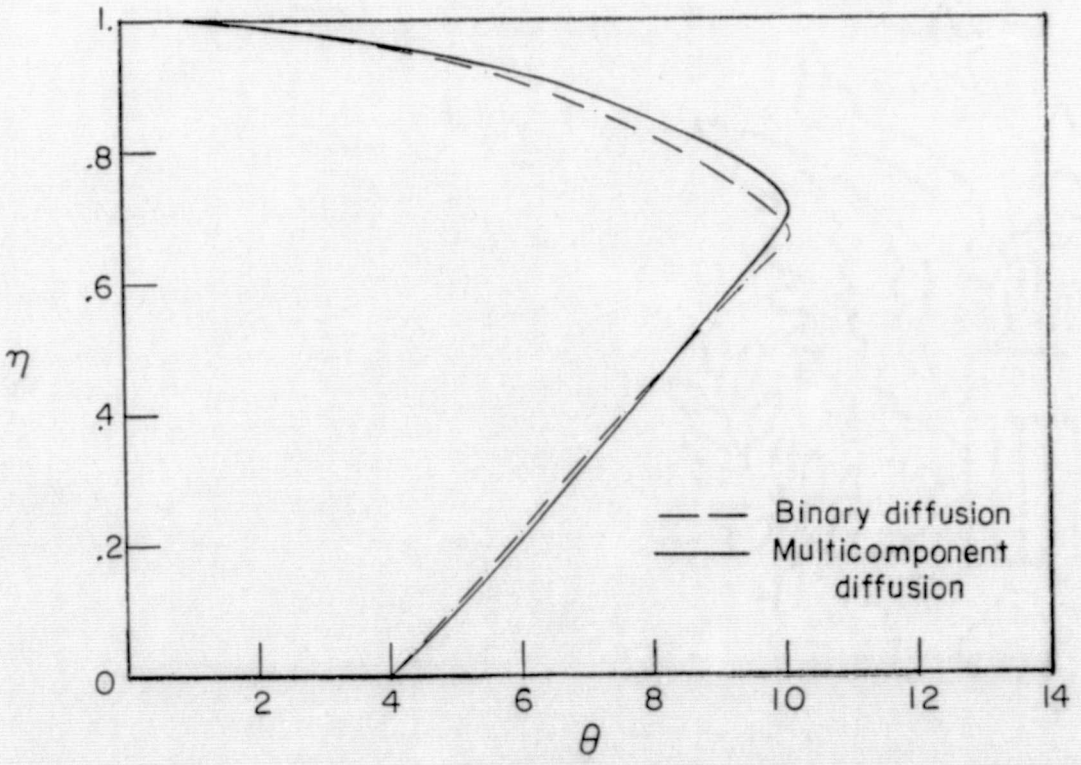

(b) $\delta_o = 0.5$

Figure 17.- Temperature profiles for $\delta_o = 0.75$ and 0.5.

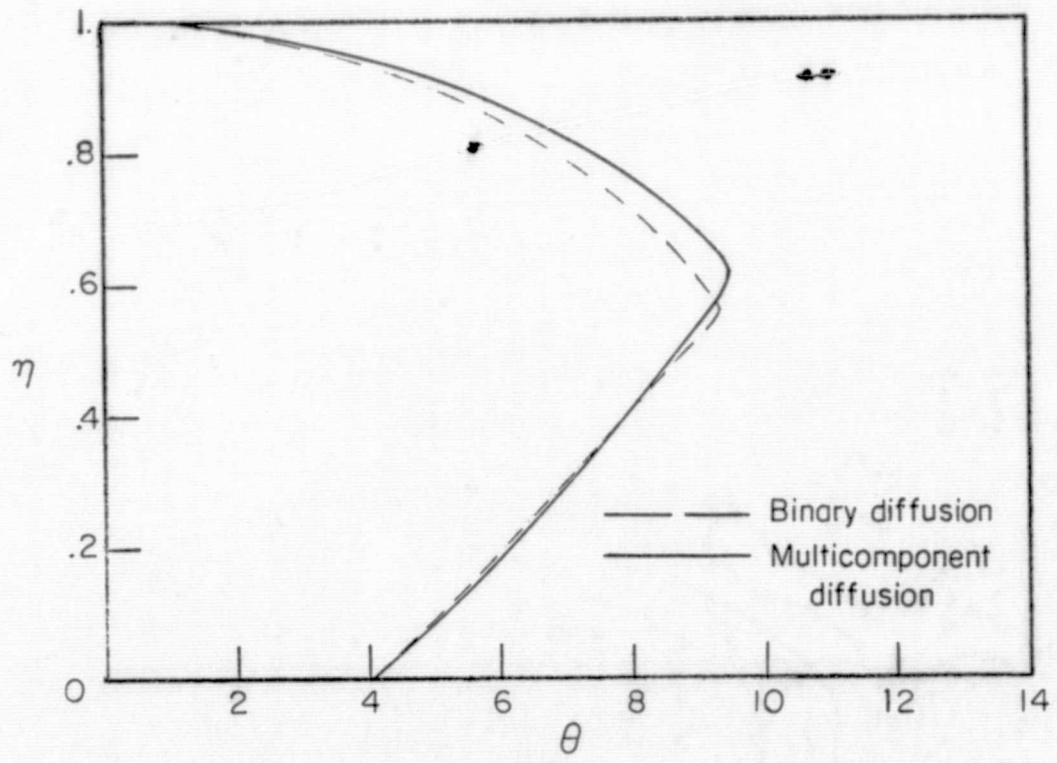

(a) $\delta_o = 0.35$

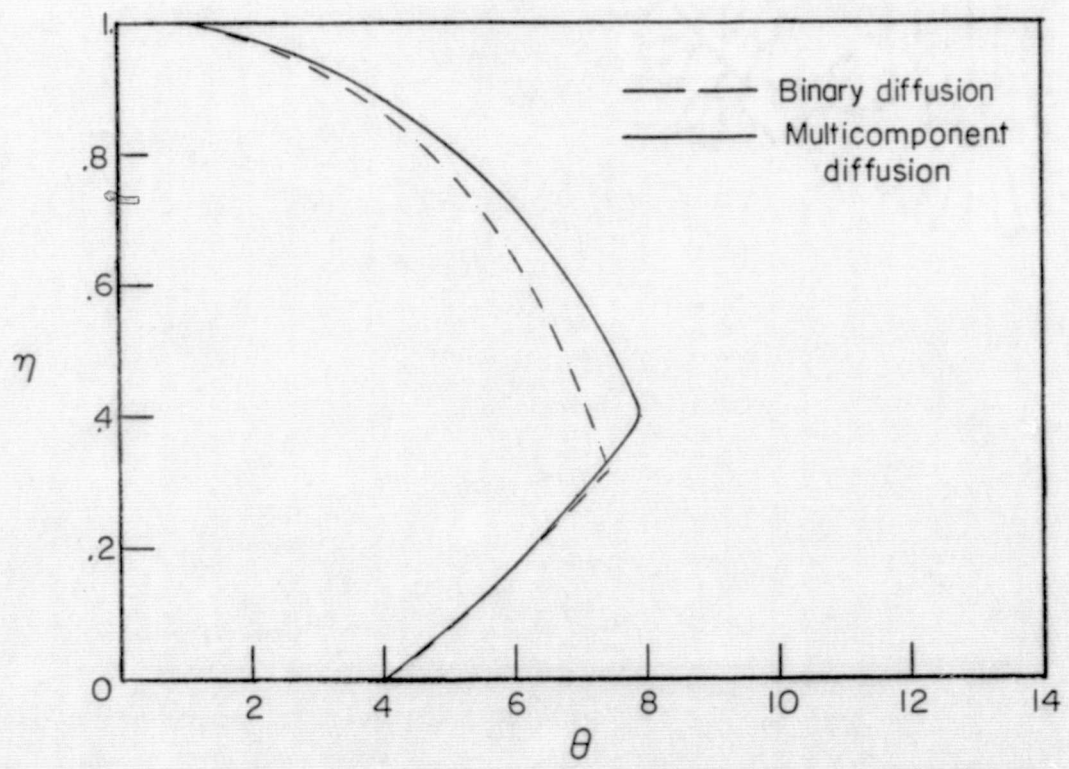

(b) $\delta_o = 0.2$

Figure 18.- Temperature profiles for $\delta_o = 0.35$ and 0.2.

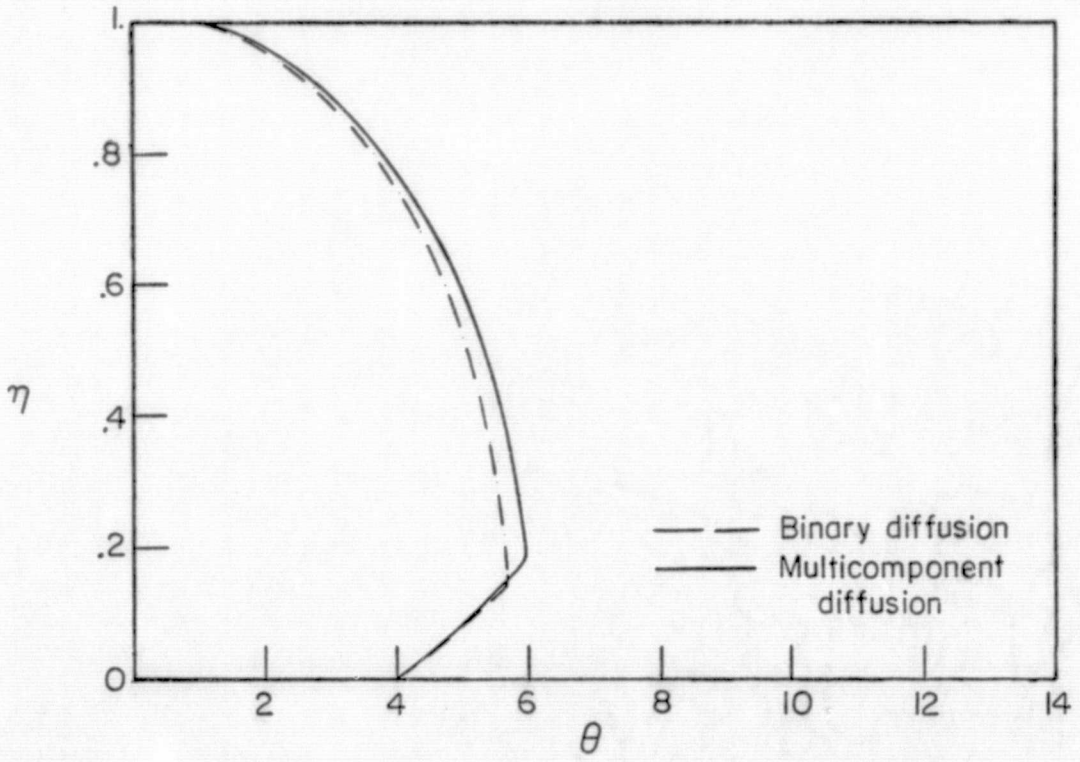

(a) $\delta_o = 0.13$

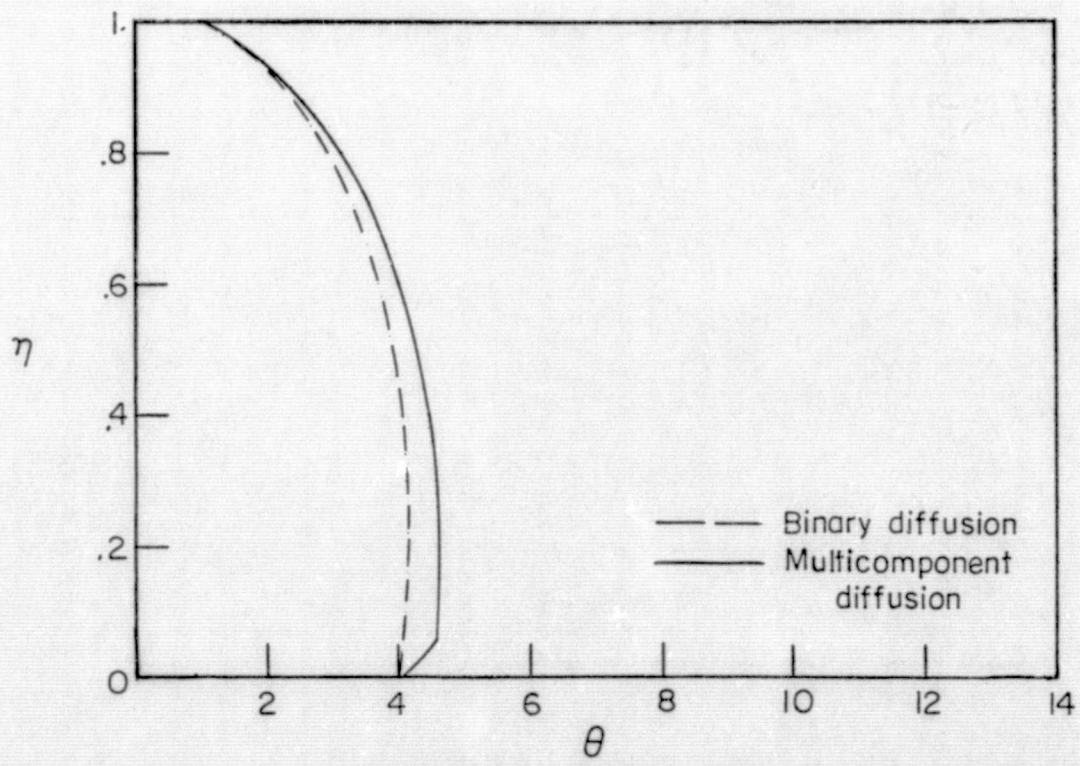

(b) $\delta_o = 0.1$

Figure 19.- Temperature profiles for $\delta_o = 0.13$ and 0.1.

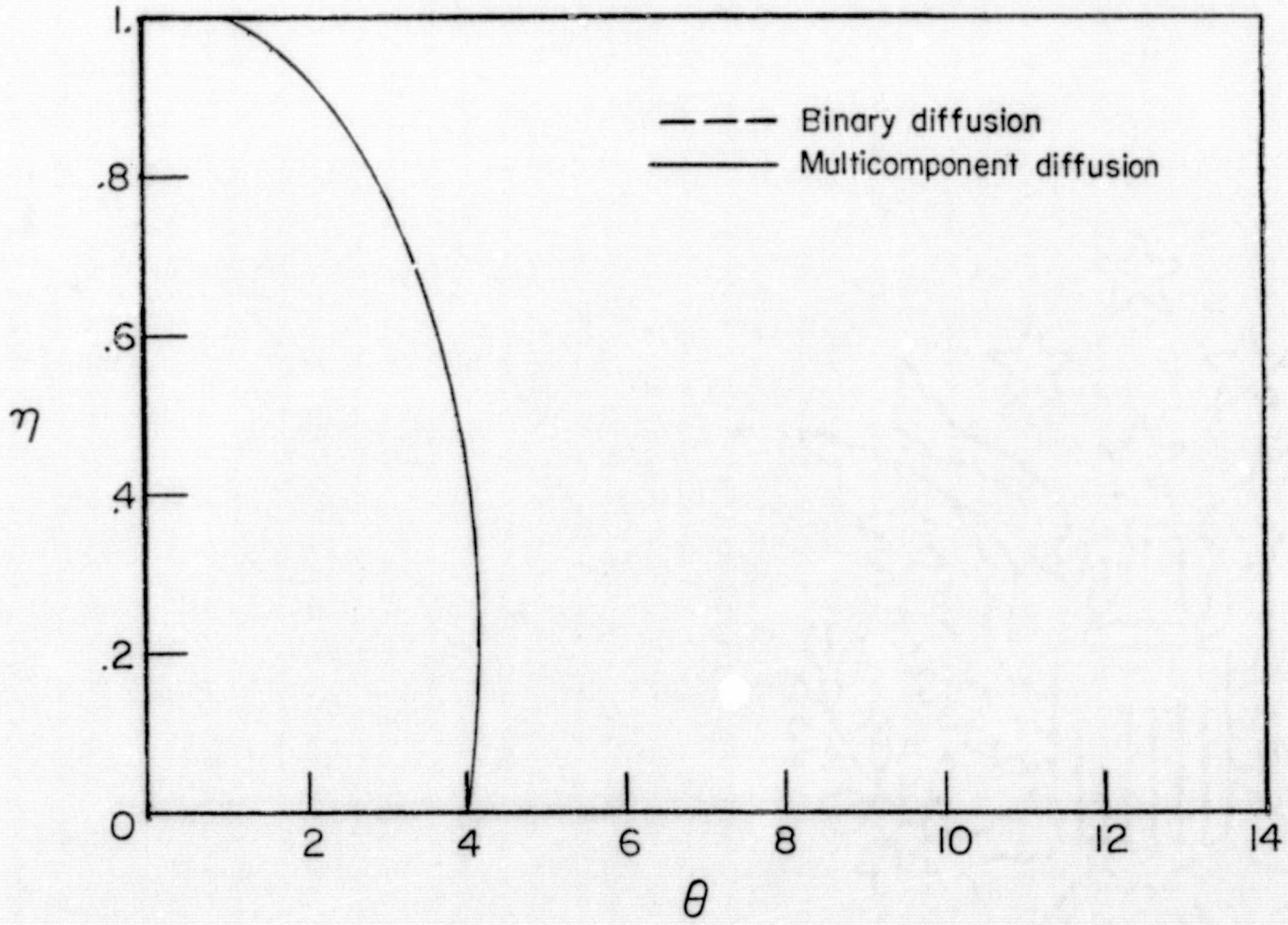

Figure 20.- Temperature profiles for $\delta_o = 0.05$.

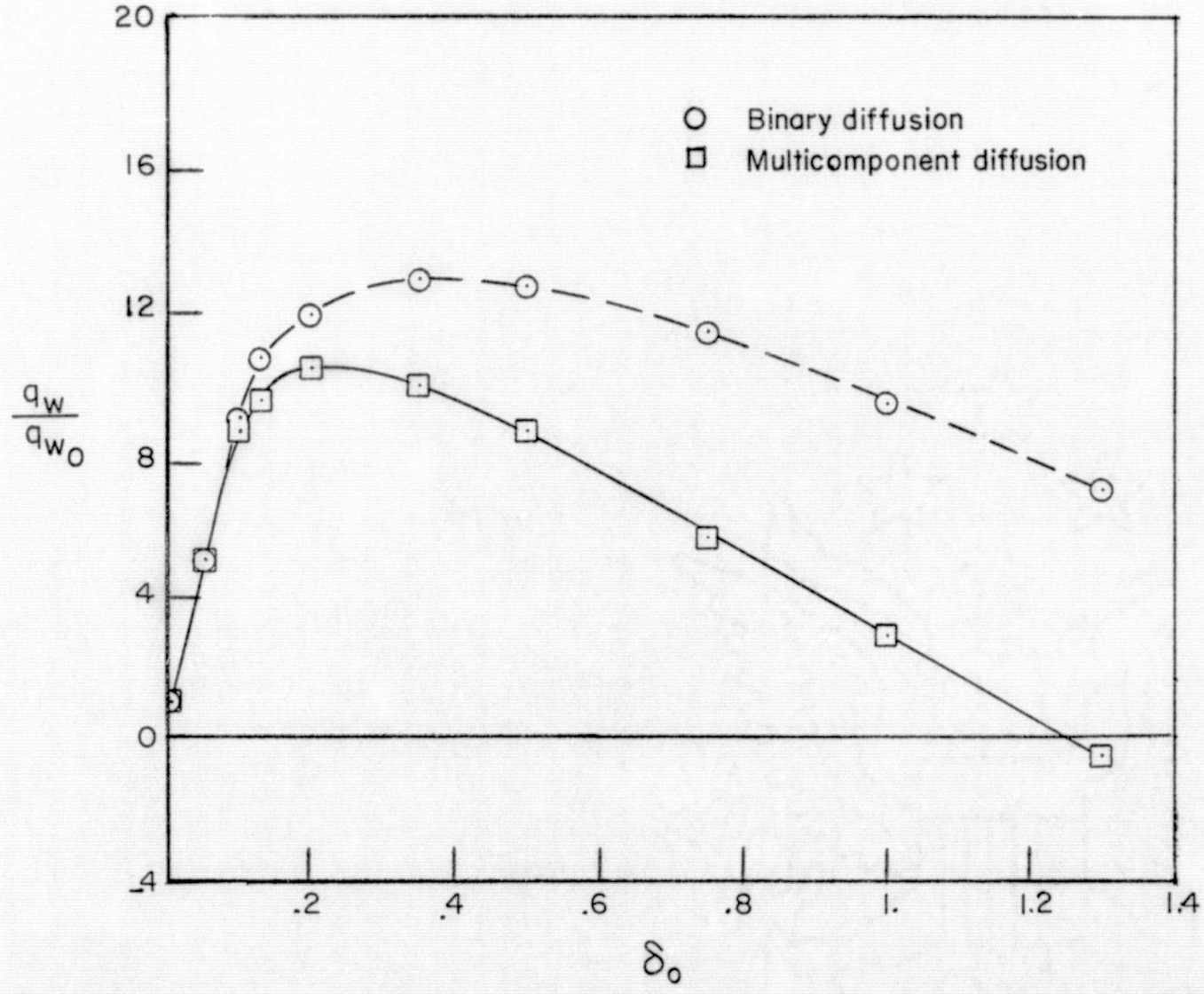

Figure 21.- Heating rate results.

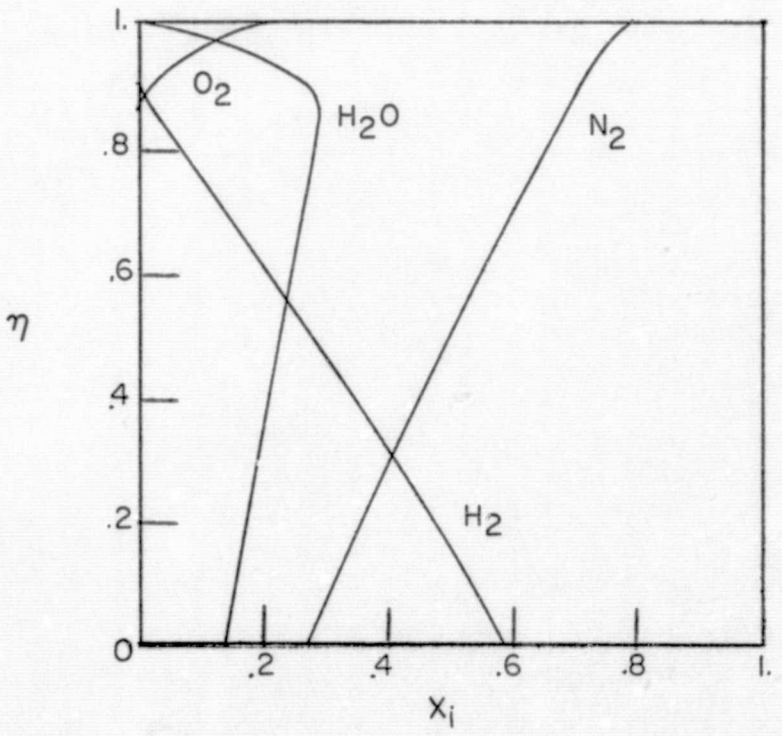

(a) Multicomponent diffusion

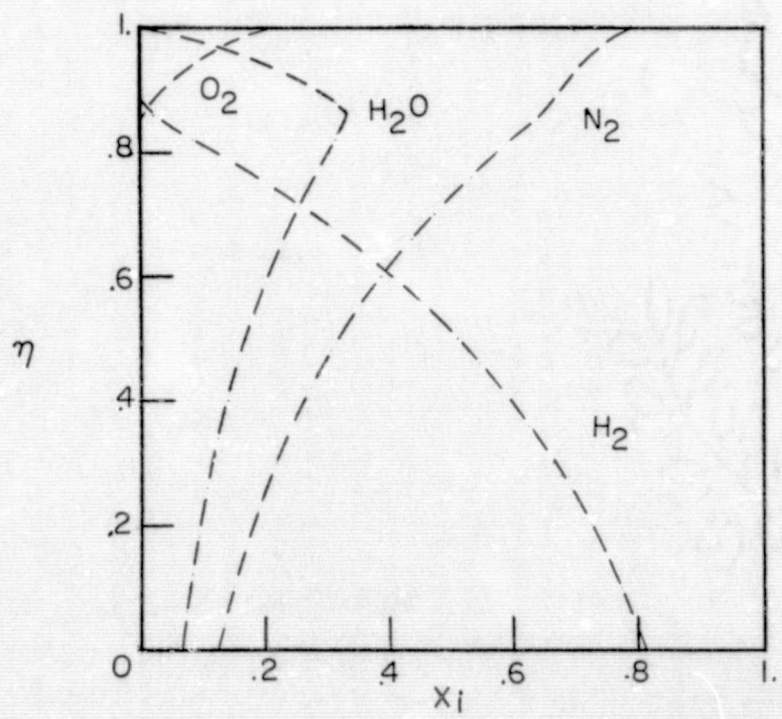

(b) Binary diffusion

Figure 22.- Concentration profiles for $\delta_o = 1.3$.

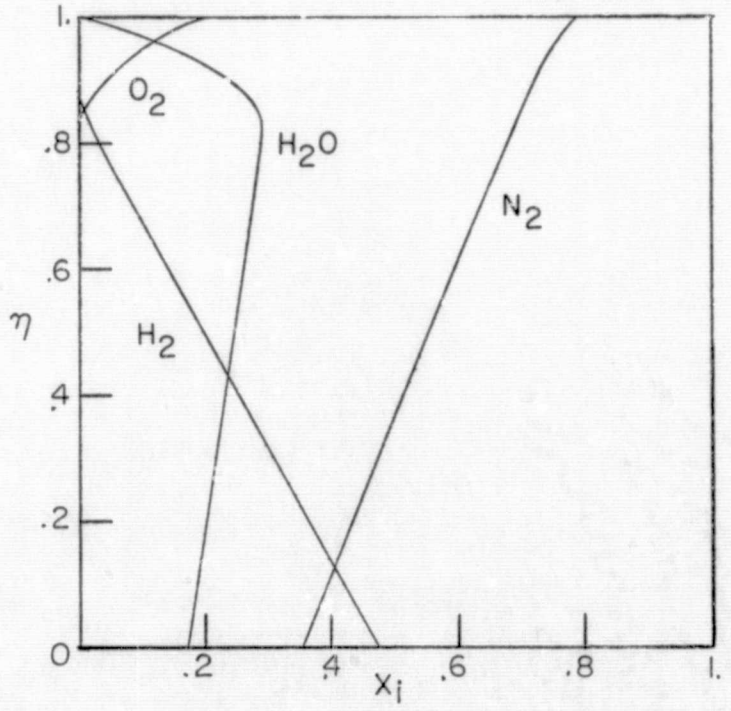

(a) Multicomponent diffusion

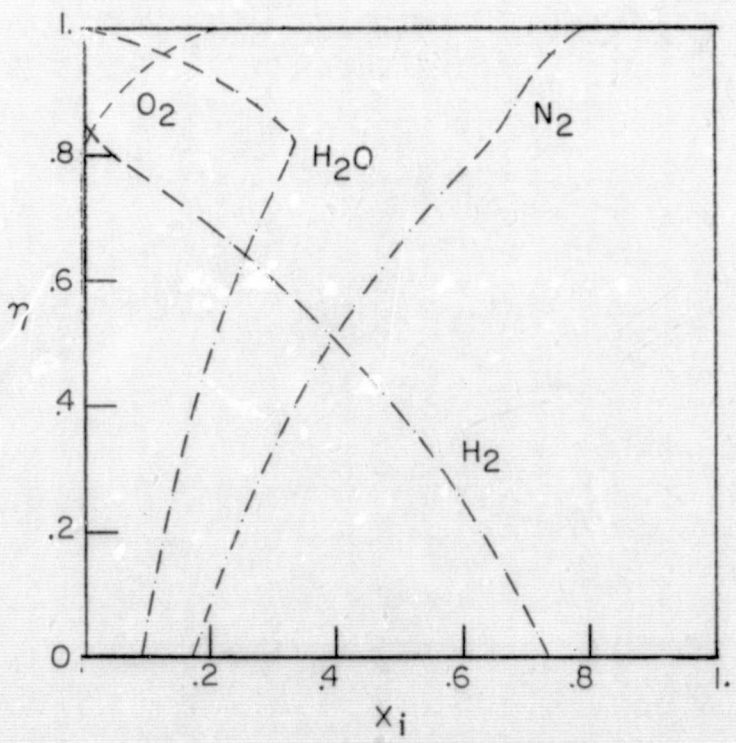

(b) Binary diffusion

Figure 23.- Concentration profiles for $\delta_o = 1.0$.

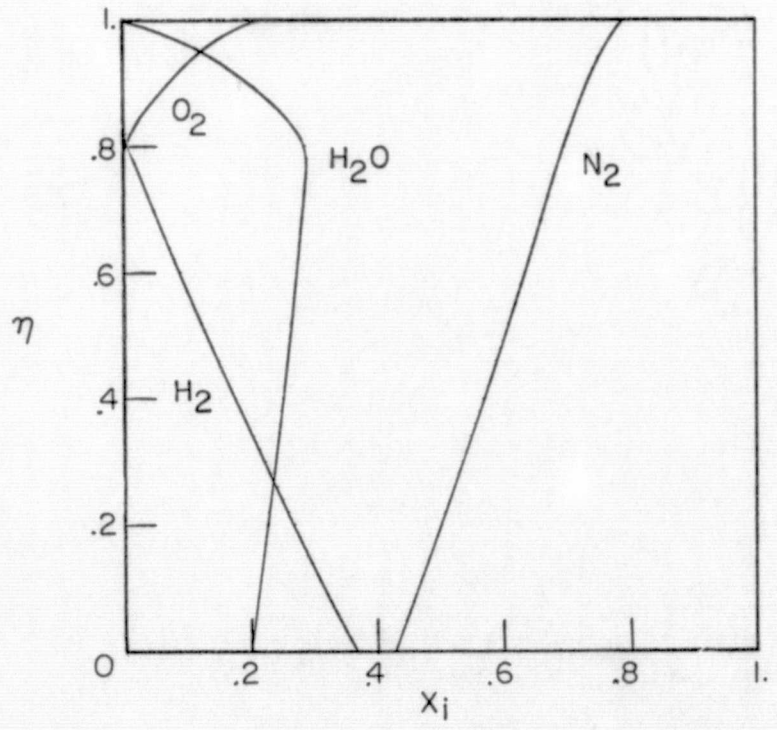

(a) Multicomponent diffusion

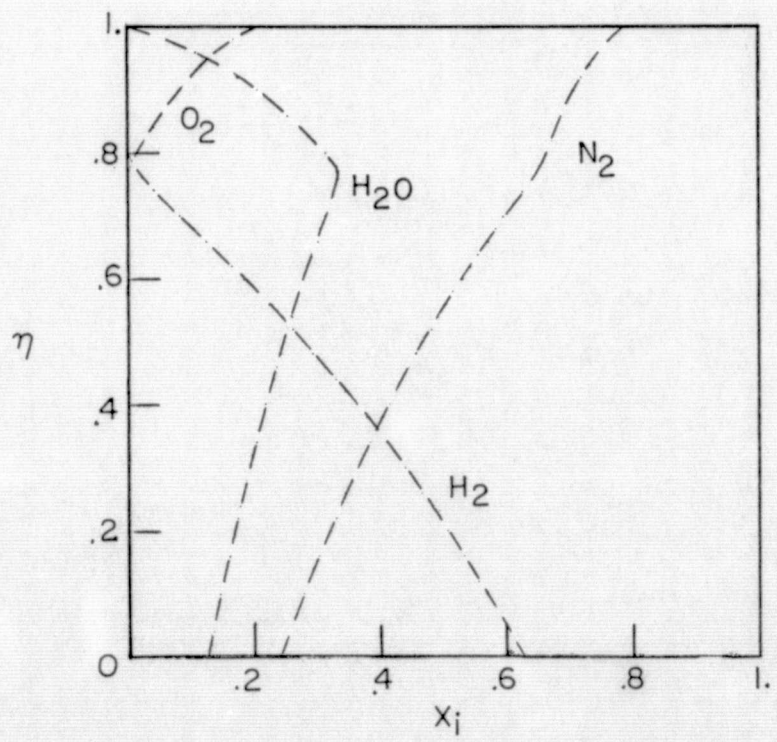

(b) Binary diffusion

Figure 24.- Concentration profiles for $\delta_o = 0.75$.

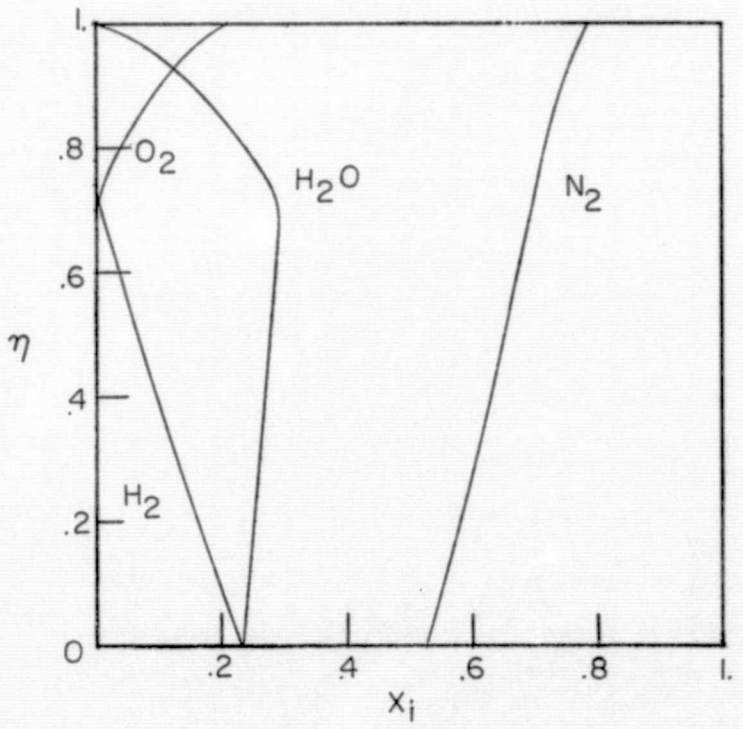

(a) Multicomponent diffusion

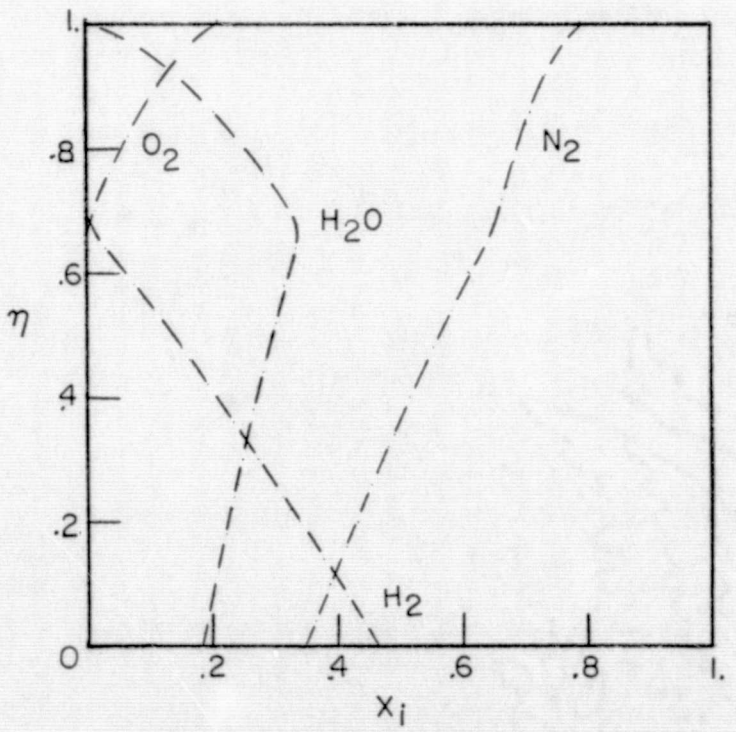

(b) Binary diffusion

Figure 25.- Concentration profiles for $\delta_o = 0.5$

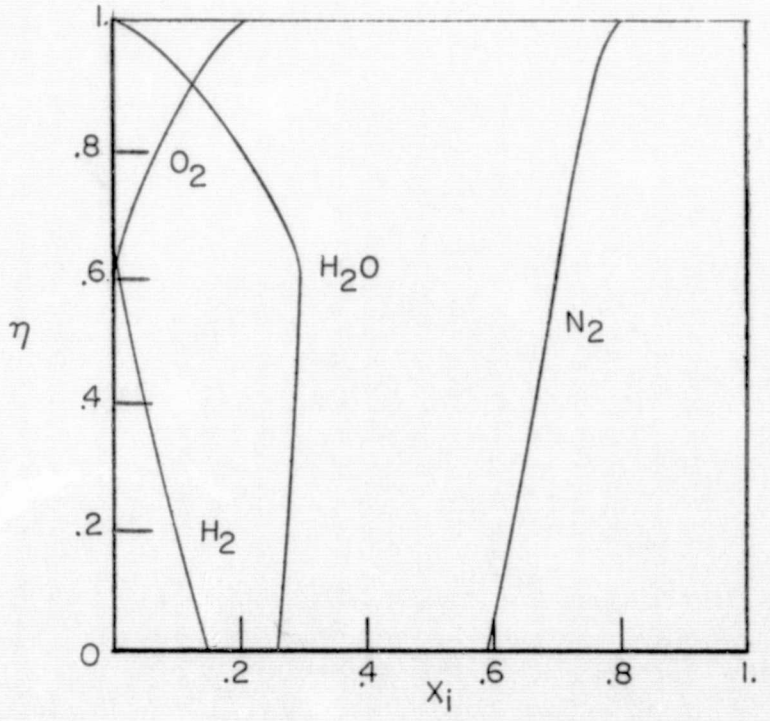

(a) Multicomponent diffusion

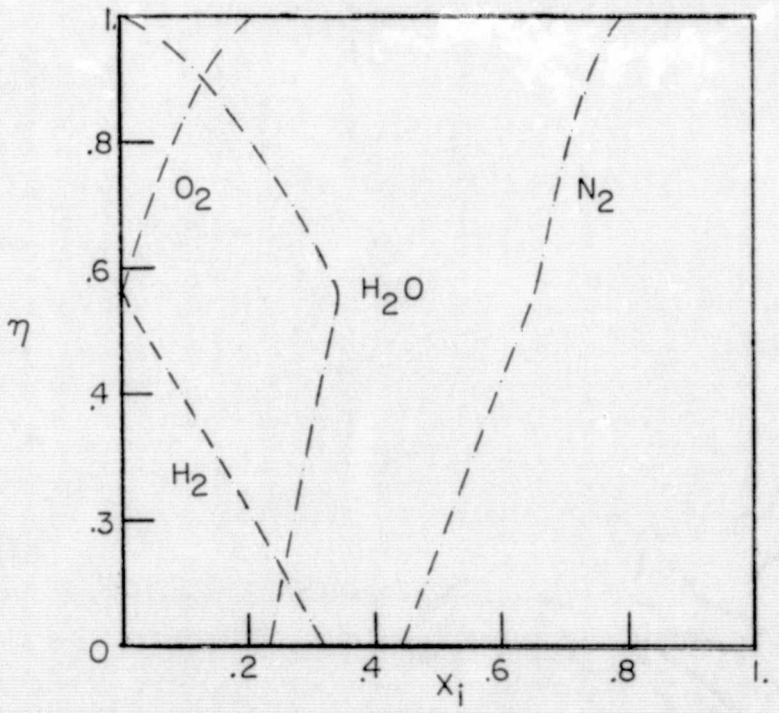

(b) Binary diffusion

Figure 26.- Concentration profiles for $\delta_o = 0.35$.

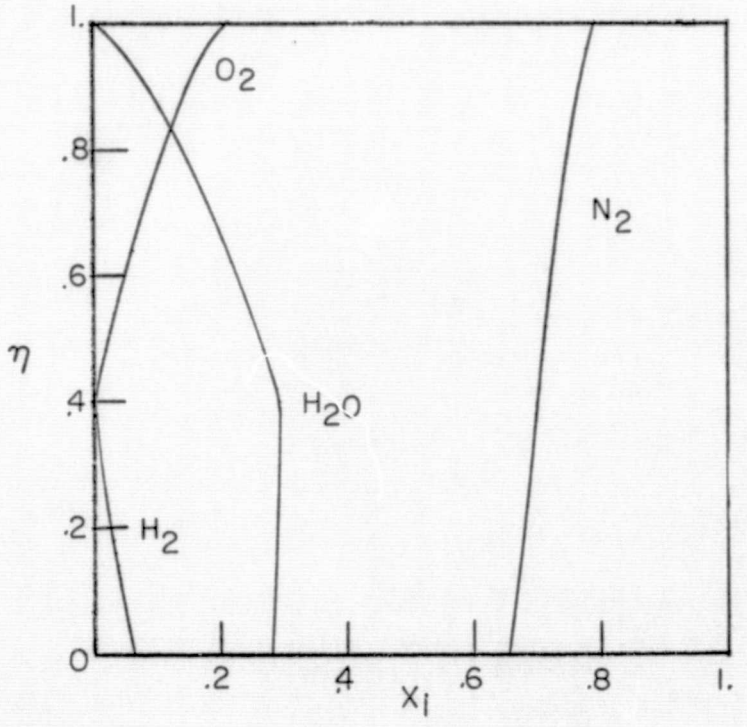

(a) Multicomponent diffusion

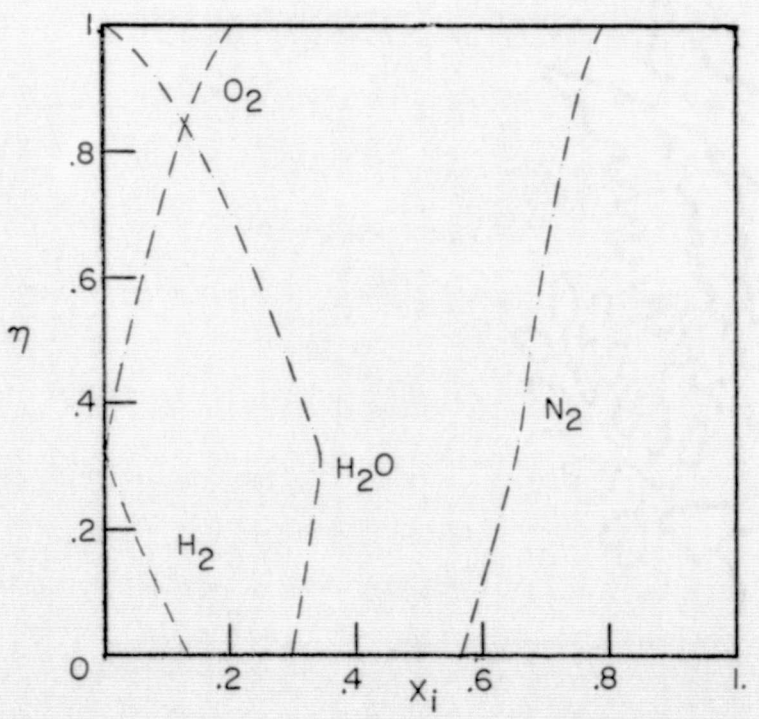

(b) Binary diffusion

Figure 27.- Concentration profiles for $\delta_o = 0.2$.

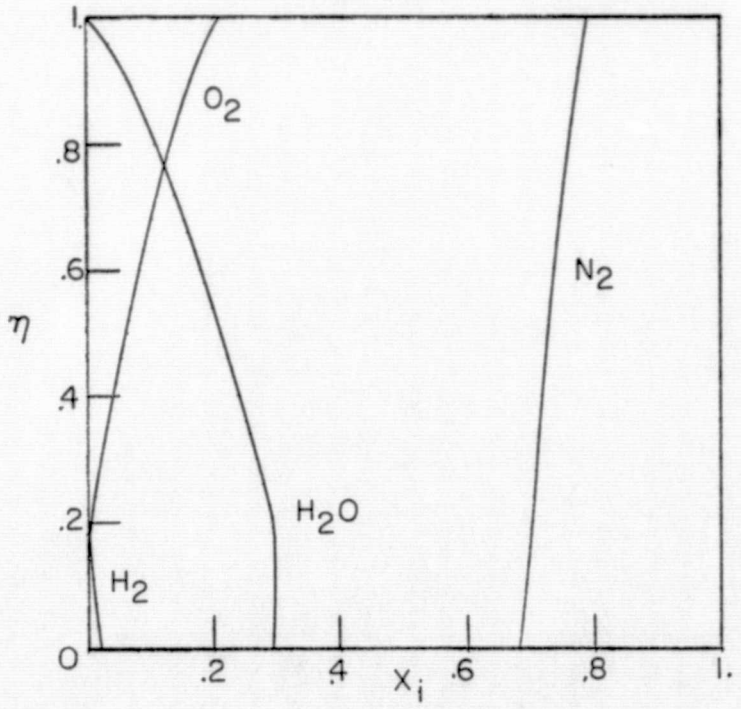

(a) Multicomponent diffusion

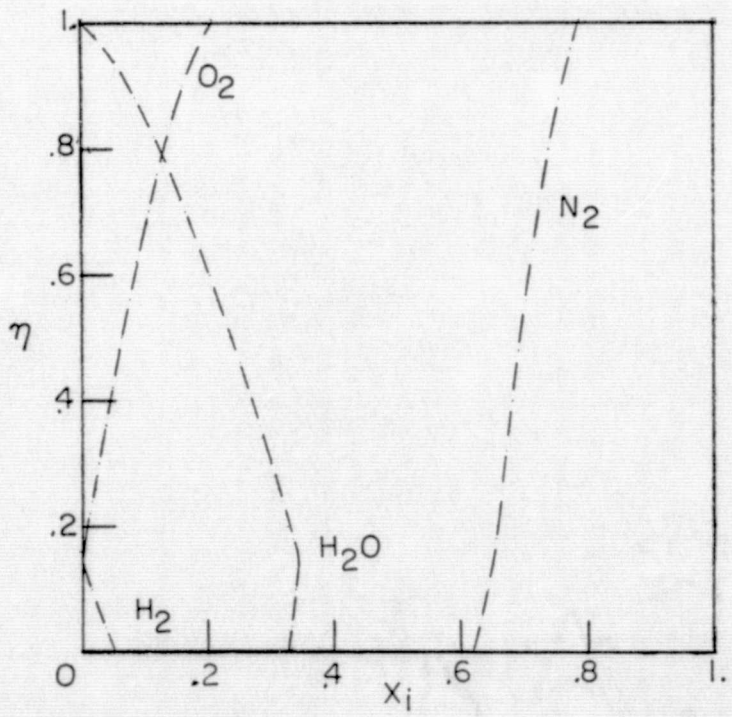

(b) Binary diffusion

Figure 28.- Concentration profiles for $\delta_o = 0.13$.

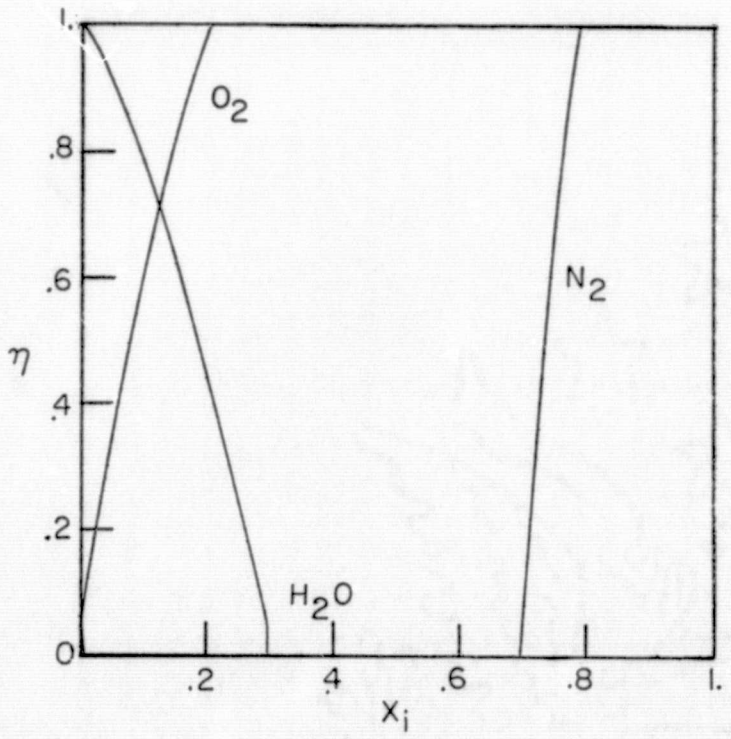

(a) Multicomponent diffusion

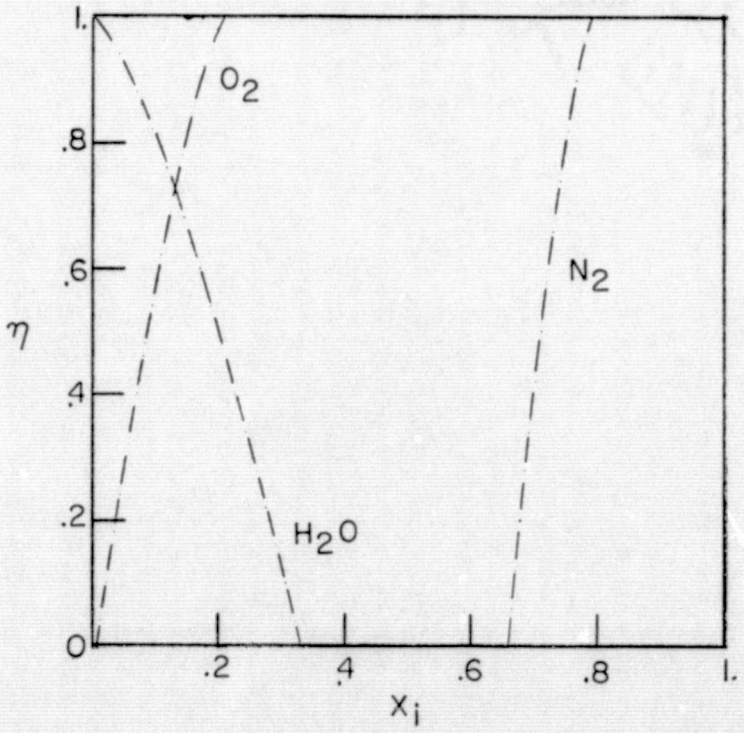

(b) Binary diffusion

Figure 29.- Concentration profiles for $\delta_o = 0.1$.

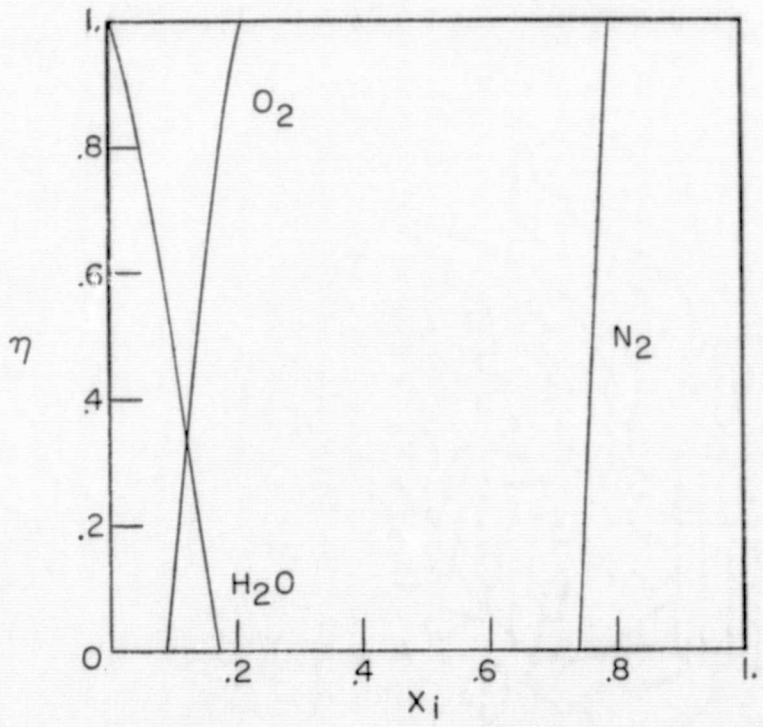

(a) Multicomponent diffusion

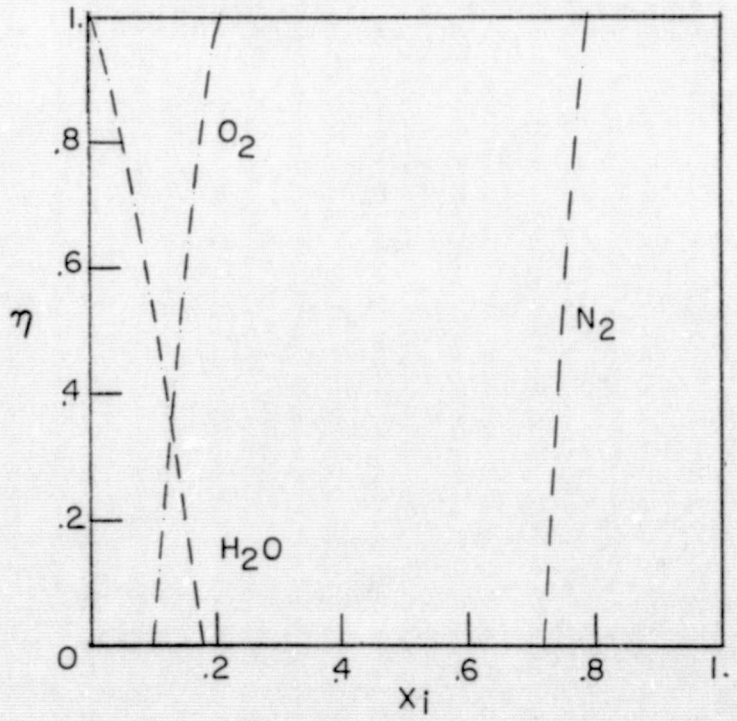

(b) Binary diffusion

Figure 30.- Concentration profiles for $\delta_o = 0.05$.

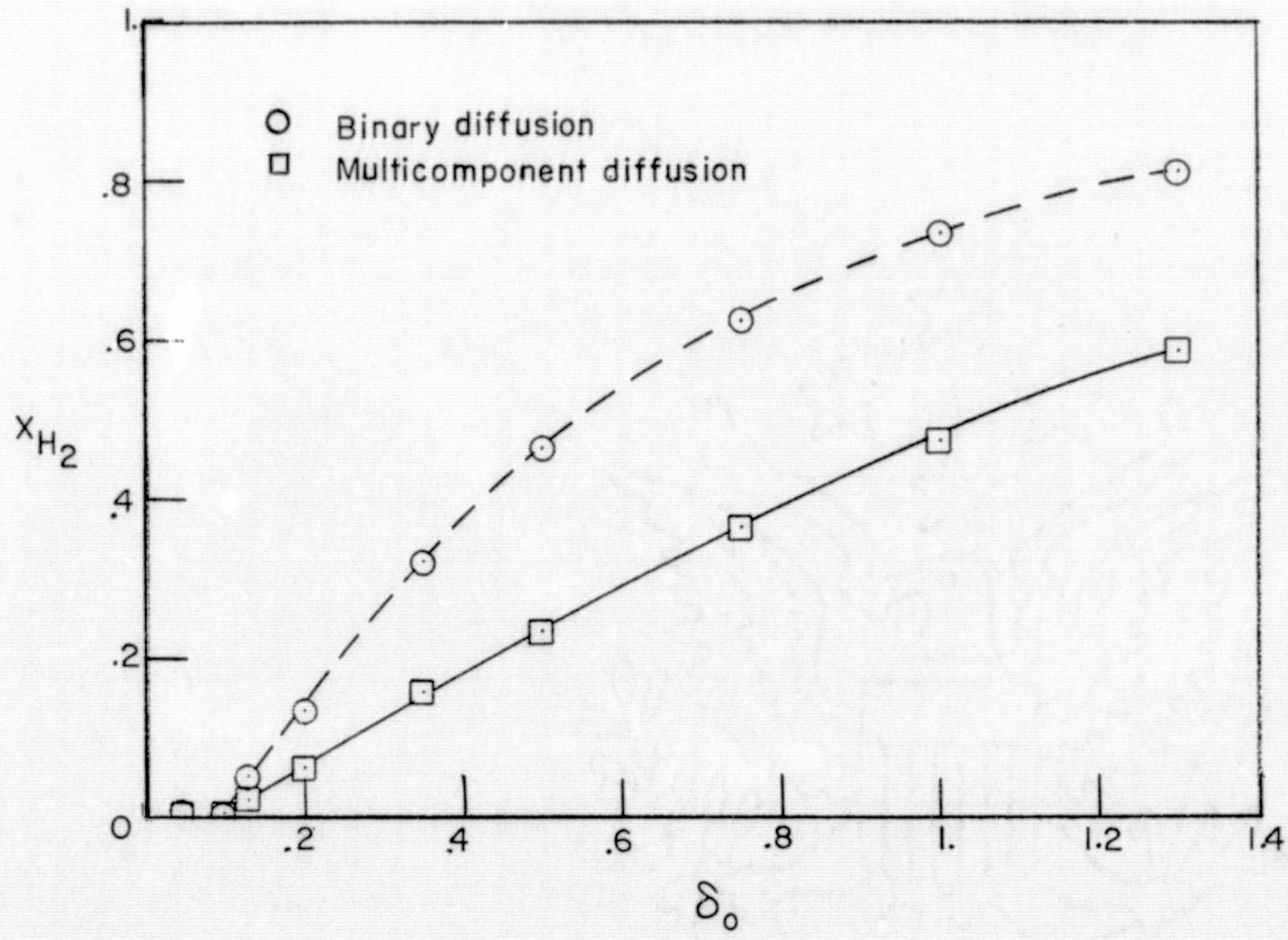

Figure 31.- Concentration of hydrogen at lower wall.

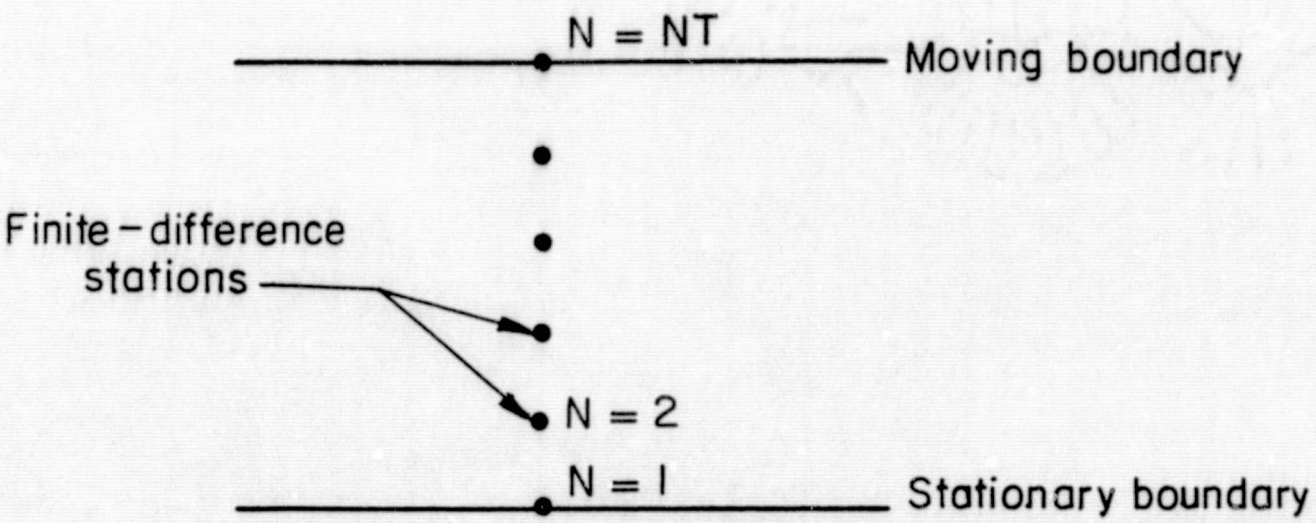

Figure 32.- Finite-difference stations.

TABLE I.- COMPARISON OF EQUILIBRIUM CHEMISTRY RESULTS

Temp.	1000		2000		3000		4000	
	Ref. 8	Present method	Ref. 8	Present method	Ref. 8	Present method	Ref. 8	Present method
h	123	123	419.8	420.0	740.8	740.9	1093.7	1094.5
C_{PR}	0.2800	0.2799	0.3091	0.3088	0.3379	0.3382	0.3561	0.3566
X_{H_2}	0	0	0.00002	0.00002	0.00276	0.00277	0.01653	0.01659
XH_2O	0.02967	0.02961	0.02965	0.02959	0.02686	0.02679	0.01289	0.01278
X_{N_2}	0.77885	0.77886	0.77884	0.77885	0.77777	0.77778	0.77241	0.77240
X_{O_2}	0.19148	0.19153	0.19149	0.19153	0.19260	0.19265	0.19817	0.19823

<u>Units</u>

h = Cal/gm

C_{PR} = Cal/gm-^{o}K

T = ^{o}K

<u>Initial conditions</u>

p = 1 atm

$\tilde{K}_O$ = 0.2318

$\tilde{K}_H$ = 0.0021

$\tilde{K}_N$ = 0.7661

TABLE II.- MOLECULAR CONSTANTS

Species	ϵ/K	σ	M
O_2	106.7	3.467	32.00
H_2	59.7	2.827	2.016
H_2O	809.1	2.641	18.02
N_2	71.4	3.798	28.02

Units

M = $gm/_{gm\text{-}mole}$

σ = angstrom